

Chapter 5 - Boundary Physics

5.1 Executive Summary.....	5.2
5.1.1 LLD program and fueling program.....	5.5
5.1.2. SOL turbulence and width program.....	5.15
5.1.3. ST divertor physics and heat flux control.....	5.23
5.2 H-mode pedestal, ELMs, and power threshold	5.33
5.2.1. H-mode Pedestal and ELM physics.....	5.33
5.2.2. L-H threshold physics.....	5.44
References.....	5.48

This page intentionally left blank

Chapter 5 - NSTX Boundary Physics 5 year plan

NSTX Boundary Physics Group

5.1 Executive Summary

Boundary physics research in NSTX is geared toward 1) continued development and improvement of NSTX operational scenarios, 2) development of the physics basis for future STs, 3) contribution to toroidal confinement physics, e.g. by comparison with high aspect ratio tokamaks, and 4) direct contributions to ITER R & D needs. Nearly all of the main upgrades in this five-year plan represent opportunities to enhance our boundary physics understanding: 1) the Liquid Lithium divertor (LLD) and core fueling program represents a bold idea to control plasma-wall interactions; 2) the center stack upgrade with higher I_p and B_t will enable access to lower v_e^* than presently available; 3) enhancements to the EFCC/RWM capabilities enable extra flexibility to understand and control the H-mode pedestal and edge localized modes; and 4) the second NBI system (for which preparations are being made in this plan) enables studies of plasma-wall interactions at peak heat fluxes beyond ITER and toward DEMO.

The second NBI and the center stack upgrade represent not only opportunities but also responsibilities, in that the high levels of heat flux and intense plasma-wall interaction must be managed for time scales ~ 5 sec, nearly tripling today's longest NSTX discharges of 1.8 sec. The combination of these facility enhancements will enable access to even lower v_{\square}^* (e.g. Fig. 5.0.1) and longer SOL connection length

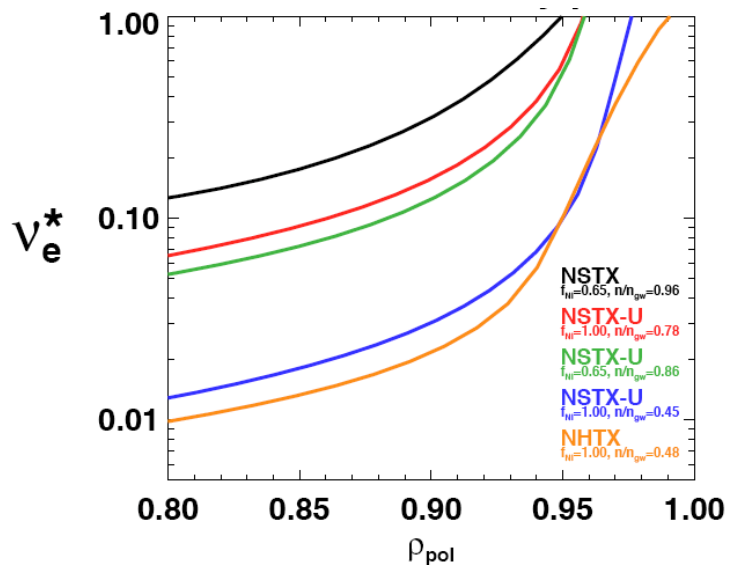


Fig. 5.0.1- Comparison of predicted edge electron collisionality v_e^* for present NSTX, NSTX-U (center stack + 2nd NBI) at two n/n_{GW} and NHTX.

for more detailed SOL width and heat flux management studies. Quantitatively the v_{\square}^* in the edge region is predicted to drop up to an order of magnitude, and within a factor of 2 of the level predicted for NHTX.

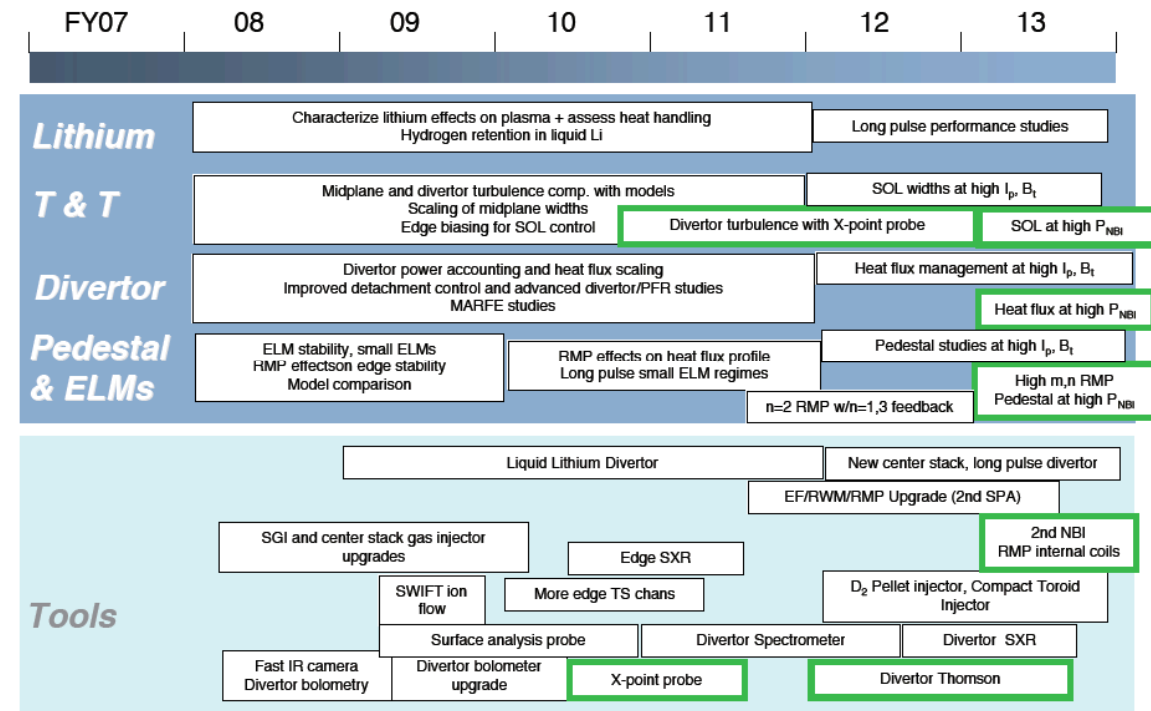
A new long pulse divertor will be designed to handle the longer pulse length enabled by the center stack and higher heating power provided by the 2nd NBI. The highest peak heat flux observed in NSTX is $\sim 10 \text{ MW/m}^2$, although up to 15 MW/m^2 has been transiently seen. For the present outer divertor ATJ graphite tiles, this range of peak heat flux translates into a maximum pulse length of 2-3 sec. before a $1200 \text{ }^\circ\text{C}$ administrative limit on PFC surface temperature would be exceeded. Moreover the scrape-off layer (SOL) heat flux width could well shrink at the lower v^* from higher I_p , B_t , and P_{NBI} values, i.e. the peak heat flux could be even higher, necessitating a new divertor implementation. To manage these levels of heat flux, double-null configuration, large flux expansion, and detachment may all be needed, and novel divertor schemes (e.g. X-divertor, super X-divertor, or snowflake divertor) may also be required.

At the highest level, the boundary program has a SOL/divertor physics component and an H-mode physics component. The first area is discussed below in the context of several themes: lithium and fueling research, SOL transport and width research, and divertor physics research with an emphasis on heat flux management. The second area is discussed in the context of two themes: pedestal and ELM research, and H-mode operational window research, with an emphasis on power threshold studies. Progress in all of these areas relies both on the facility upgrades discussed above and a set of diagnostic upgrades, listed below and discussed in detail in the following sections:

1. LLD diagnostics in the toroidal gaps between LLD segments, including thermocouples, Langmuir probes, and a two-color IR measurement
2. A divertor bolometer upgrade
3. Additional Thomson channels near the pedestal and separatrix
4. A divertor spectrometer
5. A high-resolution edge soft X-ray system for fast T_e profiles
6. A Ly- α detector array
7. A DiMES-like surface analysis probe

8. A divertor soft X-ray system for fast T_e profiles
9. An X-point reciprocating probe (incremental)
10. A divertor Thomson scattering system (incremental)

The overall time-line of the boundary physics program is shown below.



* incremental budget needed

Sec. 5.1.1 – LLD program and fueling program

1. Introduction

High-performance, long-pulse NBI-heated small-ELM H-mode plasma discharges have been developed in NSTX as prototypes for confinement and current drive extrapolations to future spherical tori¹, but these exhibit a secular density rise. A critical issue for the achievement of sustained non-inductive current drive H-mode plasmas is the control of this density rise and impurity influx. Lithium as a plasma-facing component (PFC) has potential for providing particle pumping because of its ability to pump hydrogen and reduce oxygen because of its high chemical reactivity. Given the preliminary success of lithium coatings for wall pumping, additional fueling mechanisms will be implemented to provide density control. Each of these elements: pumping and fueling, are described sequentially in this section.

Experiments to date have demonstrated improvements in plasma performance with lithium PFC's²⁻⁶, but they have primarily focused on limiter tokamak discharges in the low confinement mode (L-mode). However, future devices on the fusion energy development path such as ITER and DEMO are divertor machines. The efficacy of lithium as a PFC in divertor plasmas in the high confinement mode (H-mode) thus needs to be determined, and NSTX provides a unique opportunity for such research. The evaluation of lithium in NSTX has been conducted in a phased, three-part program to investigate density and impurity control through 1) lithium pellet injection, 2) evaporative lithium coatings on PFC's, and 3) a liquid lithium divertor. If successful, the achievement of low edge collisionality and improved confinement with lithium PFC's in NSTX would lead to a more thorough and favorable extrapolation to next-step STs and magnetic fusion energy devices in general.

Present options for fueling long pulse discharges include conventional gas puffing, high-velocity cryogenic fuel pellets, and compact toroids (CTs). Because of its technical simplicity, gas injection at the plasma edge is universally used for fueling of high-temperature plasmas in present day devices. As in high aspect ratio tokamaks, the gas fueling operating range in NSTX is defined by plasma operational limits and the injector poloidal location. The low density operational limit is determined by the onset of

a locked mode due to error fields or reconnection events, and by large type I ELMs in NBI-heated H-mode plasmas. The upper gas fueling limit is set by the onset of disruptive MHD modes, sawteeth, and confinement degradation. An additional operational constraint is H-mode access.

Gas fueling has well-known shortcomings: the low fueling efficiency (between 1 - 20 %), and gas loading of in-vessel surfaces leading to uncontrolled fueling of plasma by out-gassing and recycling. Supersonic gas injection offers improved fuel control and enhanced fueling efficiency, as compared with standard gas puffing. Pellets are commonly used in present day devices for core fueling, while CTs have been tested with some success on a few devices.

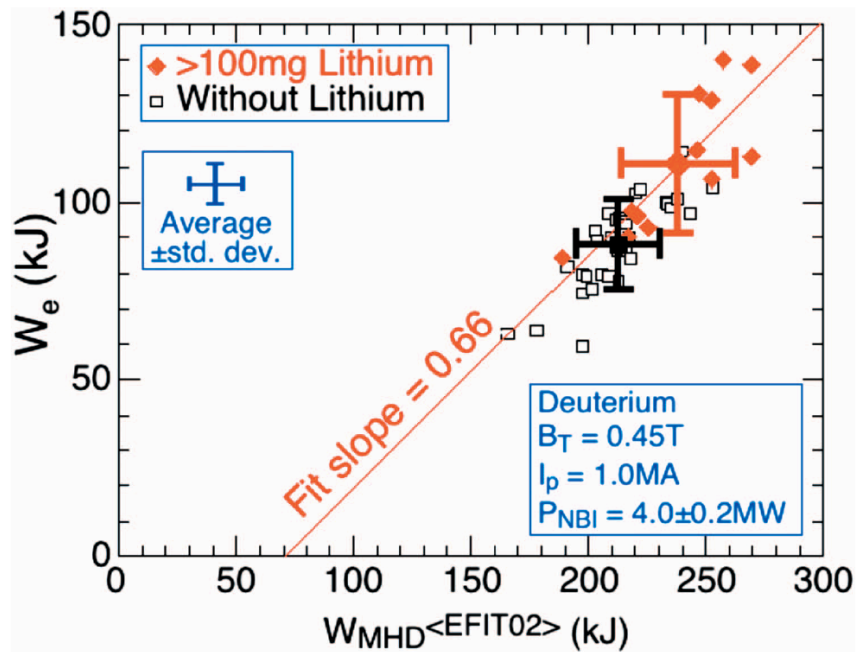


Fig. 5.1.1.1- L1 surface coatings improved plasma stored energy, mainly through electron channel.

2. Background and Results

Lithium wall coating results

Recent NSTX experiments have shown significant and recurring benefits of lithium coatings on PFC's to the performance of divertor plasmas in both L- and H- mode confinement regimes heated by high-power neutral beams⁷. In 2005, a reduction in recycling was achieved in NSTX plasmas with lithium pellet injection (LPI). Low-Lithium pellets in the range of 2 to 5 mg were injected into both limiter and divertor plasmas. Measurements of the visible light emission from the plasma edge indicated that the injected lithium was deposited primarily in the vicinity of the discharge contact area. The first neutral beam-heated L-mode discharge that followed a discharge with LPI showed a reduction in the volume-average plasma density of about a factor 2 compared

with to a similar discharge prior to the introduction of lithium. This was also observed in higher density H-mode plasmas. While the reduction in density did not persist in subsequent discharges, there was enough of an effect to suggest that more coverage of PFC's with lithium might improve particle pumping.

During NSTX experiments in 2006 and 2007, lithium coatings were produced with a single oven mounted on the upper dome of the vacuum vessel^{7, 8}. This LITHium EvaporatoR (or LITER) directed a collimated stream of lithium vapor downwards toward the graphite tiles of the lower center stack and divertor. In 2006, lithium deposition prior to a plasma shot decreased the plasma density, inductive flux consumption, and ELM frequency and increased the electron temperature, ion temperature, energy confinement time, and DD neutron rate. In addition, extended periods of MHD quiescence were observed.

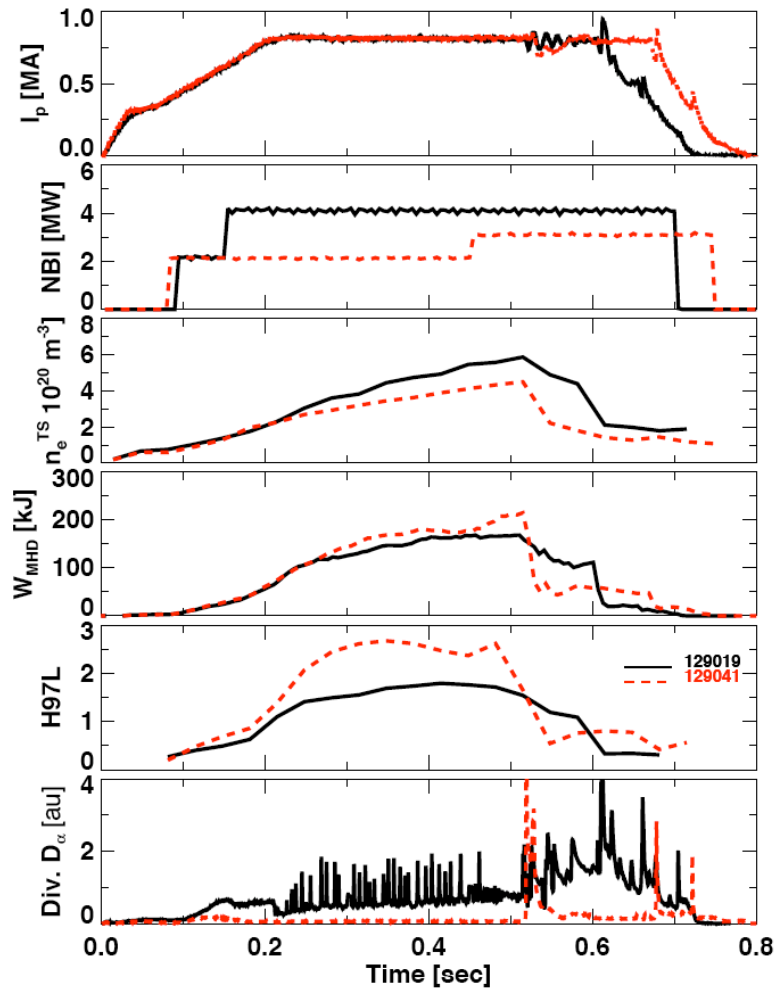


Fig. 5.1.1.2- Comparison of pre-(black) and post-LiTER(red) discharges with double LiTER system in 2008.

Measurements of the visible emission from the lower divertor also showed a reduction in the deuterium, carbon, and oxygen line emission. However, the improvements in plasma conditions were transient and performance reverted to the pre-lithium conditions by the following discharge unless the evaporation was resumed.

Erosion or passivation of the thin coating on the contact areas on the divertor by

plasma heat and particle fluxes and lithium reactions with the graphite substrate were possible explanations for the transient nature of the 2006 improvements. Such considerations motivated a LITER upgrade in 2007 to a larger diameter exit duct and improved heaters, and the re-aiming of the evaporator to increase the divertor target deposition rate by a factor of three. In addition, the 2007 LITER experiments involved continuous deposition between and during discharges. Generally both electron stored energy (W_e) and total plasma stored energy (W_{MHD}) increased following lithium deposition (Fig. 5.1.1.1). Although there is variability in the plasma performance, it is clear that both the best and the average confinement occurred after lithium and that the increase in W_{MHD} occurs mostly through an increase in W_e .

Other salient results with lithium evaporation included a broadening of the electron temperature profile, and changes in edge density gradients that benefited electron Bernstein wave coupling. Significant modifications to ELM behavior were also observed, as shown in Fig. 5.1.1.2. A reduction in ELM frequency and amplitude, followed by a period of complete ELM suppression, occurs in plasmas after lithium deposition⁸. There is a corresponding increase in W_{MHD} during the period when large ELMs are greatly reduced (0.3 - 0.5 s.). The power step from 2->3 MW in the post-LiTER discharge resulted in $\beta_N > 5.5$, i.e. the global β_N was exceeded. Keeping the NBI power fixed at 2 MW resulted in a longer discharge with a continuous increase in radiated power, owing to impurity accumulation in the ELM-free discharge.

Fueling program results

It has been demonstrated experimentally in both NSTX and MAST that H-mode plasmas fueled by a high field side (HFS) gas injector have much lower power thresholds and better reproducibility^{9, 10}. It has been suggested that the effect could be

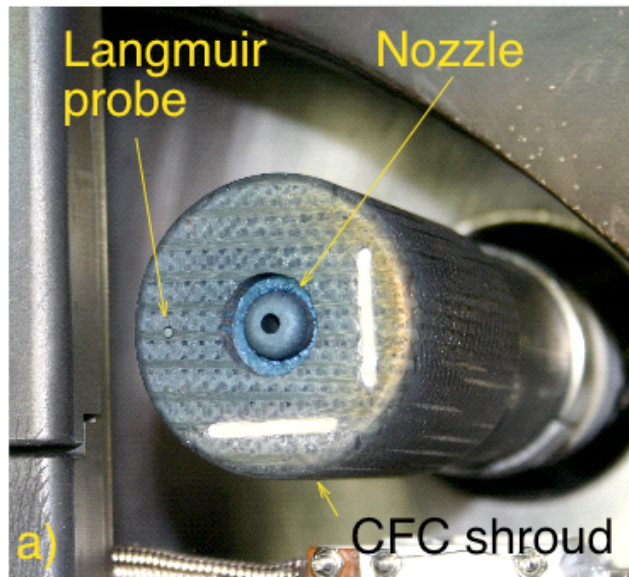


Fig. 5.1.1.3 - Photo of a supersonic gas injector inside NSTX

attributed to the charge-exchange viscous drag for neutral sources. The drag from LFS fueling is higher than from the HFS because the ions lost to charge exchange have the highest toroidal velocity at the outer midplane where the toroidal field is weakest. However the present HFS midplane injector on NSTX does not allow control of the gas flow duration, and as a result, the n_e typically increases continuously at a rate of $dN_i/dt < 7 \times 10^{20} \text{ s}^{-1}$. To address fueling efficiency and gas injection control issues, a supersonic gas injector was recently implemented.

The low field side supersonic gas injector (SGI) on NSTX consists of a small converging-diverging graphite Laval nozzle and a piezoelectric gas valve (Figure 5.1.1.3).

The nozzle is capable of producing a deuterium jet with Mach number $M=4$, estimated gas density at the nozzle exit $n \sim 5 \times 10^{23} \text{ m}^{-3}$, estimated temperature $T < 70 \text{ K}$, and flow velocity $v = 2.4 \text{ km/s}^{11-13}$. Despite the beneficial L-mode fueling experience with supersonic jets in limiter tokamaks, there is a limited experience with fueling of high-performance H-mode divertor discharges and the associated density, MHD stability, and MARFE limits¹⁴⁻¹⁶. In

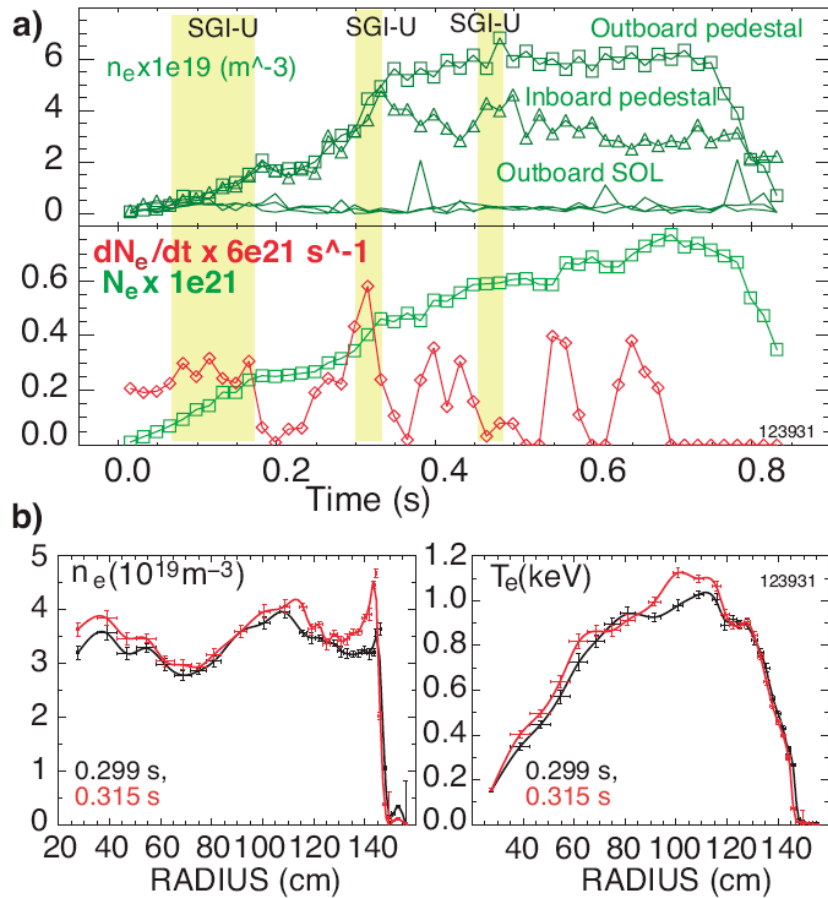


Fig. 5.1.1.4- discharge with SGI fueling: (a) inner and outer pedestal n_e , as well as outboard SOL density are shown, along with SGI pulses in yellow, and the evolution of electron inventory (N_e) and dN_e/dt ; (b) profiles of n_e and T_e before and during an SGI pulse.

initial supersonic deuterium jet fueling experiments in NSTX, a reliable H-mode access, a low NBI power threshold, $P_{LH} < 2$ MW, and a high fueling efficiency (0.1-0.4) have been demonstrated (e.g. Figure 5.1.1.4)^{17, 18}. Progress has also been made toward a better control of the injected fueling gas by decreasing the uncontrolled high field side (HFS) injector fueling rate by up to 95 % and complementing it with the supersonic jet fueling¹⁹.

3. Plans (FY09-10)

The primary goal of lithium PFC research on NSTX in FY09-10 is to investigate the effects of a liquid lithium divertor (LLD) on plasma performance, e.g. its ability to provide density control through deuterium pumping, its effect on edge/ELM stability, and its effect on electron transport and global confinement. The LLD is about 20 cm wide, and will be located on the outboard divertor (OBD) about 5 cm outboard of the gap for coaxial helicity injection (CHI) between the OBD and the inboard divertor. (toroidal view shown schematically in Fig. 5.1.1.5). The location and dimensions of the LLD were

chosen so that the density would be reduced by 50-60% in low-triangularity plasmas, and 25-30% in high triangularity plasmas (poloidal cut shown schematically in Fig. 5.1.1.6). These density reduction estimates were obtained from 0-D modeling,

2-D data constrained pumping simulations have just begun²⁰. Starting from a well documented H-mode discharge ($I_p=0.8$

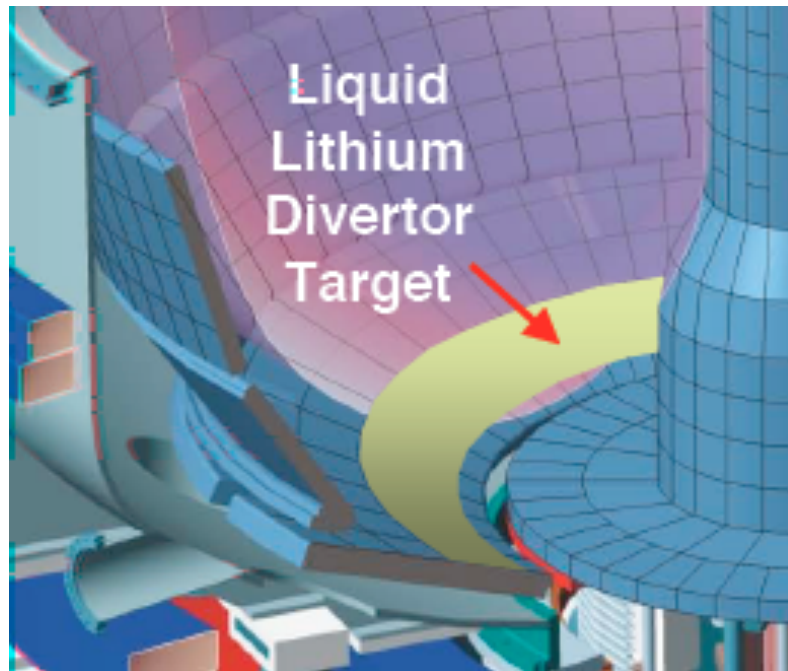


Fig. 5.1.1.5- LLD tray shown schematically as an annulus located physically on the outboard divertor. There are 4 toroidal breaks in the LLD for installation ease, and the tiles between the breaks contain many diagnostics.

MA, $B_t=0.45$ T, $P_{\text{NBI}}=1$ MW), the cross-field transport coefficients were varied to match available profiles. The recycling coefficient was then reduced to simulate the effect of lithium pumping. A strong increase in divertor T_e , decrease in divertor n_e , and a $\sim 50\%$ increase in peak heat flux was predicted (see Fig. 5.1.1.7).

Initial plans are to coat the LLD surface with lithium using the LITER evaporators. A unique feature of the LLD is that it will have heaters to maintain its temperature between 200C and 400C. This is sufficient to keep the lithium on its surface molten and actively pumping, but not significantly evaporating. Built-in thermocouple arrays (toroidal and radial) will be used to confirm the LLD temperature. The plan is to install the LLD in time for the FY 2009 run. Details on the technical design aspects are given in the chapter 7 on facility enhancements.

The LLD is a temperature-controlled copper plate with a thin stainless steel layer to protect it from the lithium. A porous molybdenum coating will be plasma-sprayed onto the stainless steel. The characteristics of LLD for particle pumping and hydrogen retention will be determined during NSTX plasma operations in FY09. It may be possible to upgrade the LLD to a version with a mesh that allows a higher lithium inventory, if offline tests of the concept are successful.

The LLD will have four toroidal segments, with graphite tiles providing breaks between these segments. The four sets of graphite tiles will contain 1) a finely spaced Langmuir probe (4mm radial separation over

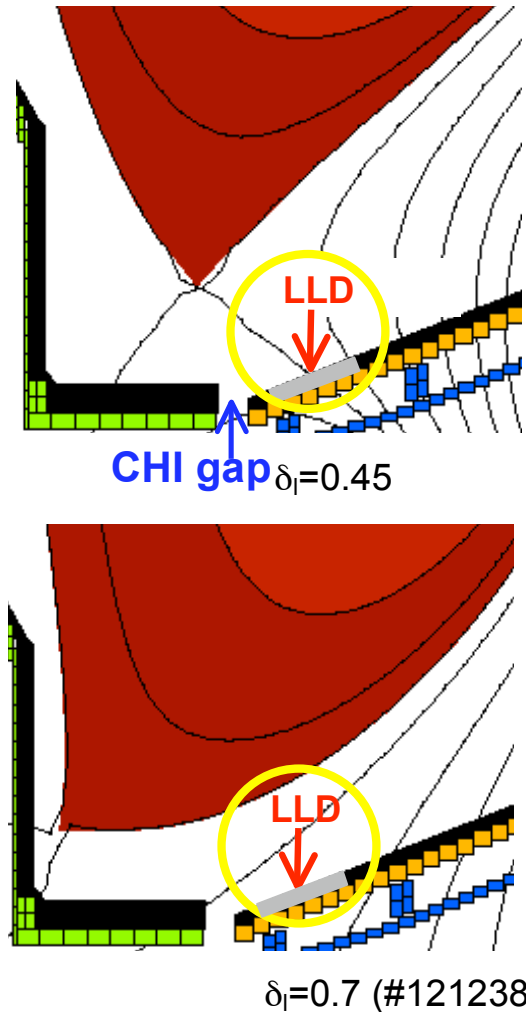


Fig. 5.1.1.6- Poloidal cut of LLD with high low δ and high δ equilibria. Calculations showed that the LLD would reduce density in these shapes by about 50% and 25%

a 10cm range), 2) magnetic probes for equilibrium reconstruction, and 3) two sets of electrodes for SOL biasing studies. In addition there will be top-down views for 1 slow IR camera (30 Hz), 1 fast IR camera (10 kHz), several 1-D linear arrays for recycling measurements, and several 2-D visible cameras to determine the impact of the LLD on divertor parameters.

LLD Plans for FY09-10 (more details given in section 5.1.3 plans):

- Install and characterize plate-based LLD operation
- Perform hydrogen retention and pumping efficiency studies, i.e. gas balance experiments
- Optimize efficiency of gas injector fueling
- Model pumping efficiency of LLD and effect on the edge and divertor plasma with DEGAS-2, SOLPS, UEDGE, and XGC codes.

New tools: LLD + diagnostics, upgraded supersonic gas injector, programmable center stack gas injector, CHERs capability to measure Li density and core concentration.

Fueling Plans for FY09-10:

Near-term plans on H-mode fueling optimization studies on NSTX include two efforts: one with HFS gas injection fueling, and one with the supersonic gas injector. Both efforts will be an integral part of the particle balance, fueling efficiency and density control studies with the LLD.

Initial work with the high field side injector in the upper corner of the machine (“shoulder”) demonstrated equally reliable H-mode access and low power threshold in shoulder-fueled H-modes in comparison with H-modes fueled from the HFS midplane

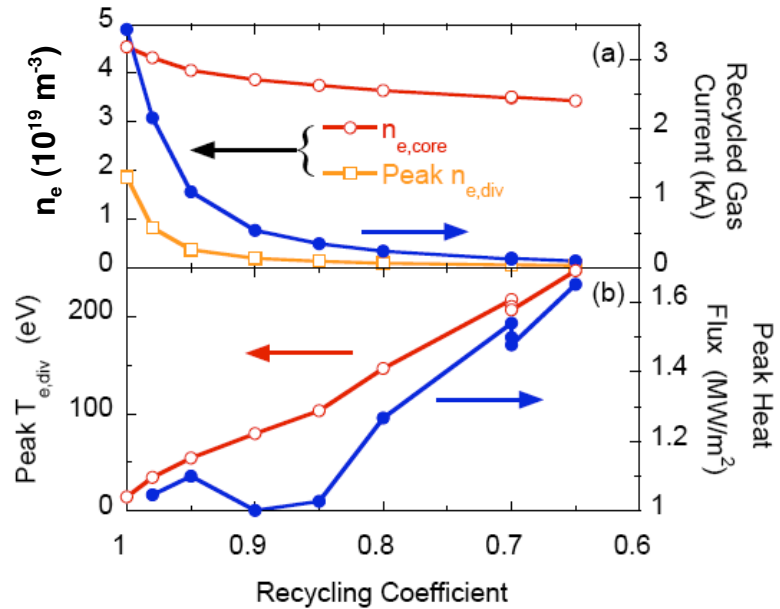


Fig. 5.1.1.7- Effect of reduced recycling coefficient on upstream ($n_{e,core}$) and divertor n_e , T_e , and q_{peak} , from a UEDGE simulation.

gas injector. We plan to implement a fully controllable shoulder gas injector, thus enabling the development of controlled HFS fueling scenarios – this is not possible for the HFS midplane injector because of limited space. Since the HFS fueling efficiency is fairly high, the goal of fueling optimization is to develop a reduced density H-mode with a possible feedback of density from the HFS shoulder injector. In addition, the supersonic gas jet is also viewed as a candidate for high-efficiency well-controlled gas fueling compatible with reliable H-mode access. The main effort will be the development of an SGI-fueled long-pulse high performance low-density H-mode plasma scenario with the locked mode correction and a density feedback algorithm with SGI.

Also, the fueling and penetration characteristics of the supersonic gas jet will be studied in detail. Specifically, we plan to carry out detailed measurements of penetration and fueling characteristics of the SGI with fast cameras, the upgraded multi-channel Far Infrared Tangential Interferometer / Polarimeter (FIRETIP) diagnostic, and the Langmuir probes. These measurements will be compared with the analytic neutral penetration model, and the DEGAS 2 neutral transport numerical model. We will try to improve the jet characteristics (density, collimation) with various supersonic nozzle designs, including the cryogenically cooled nozzle specially designed to achieve deuterium clustering. Laboratory tests will be carried out to characterize jets obtained with simple converging, conical nozzles and cryogenic nozzles. Finally, we plan to study the H-mode access and pedestal characteristics of the SGI-fueled H-modes. Specifically, the expected deeper penetration of the supersonic gas jet could change the pedestal characteristics (width, collisionality) beyond the limits defined by gas or recycling fueling.

4. Plans (FY11-13)

LLD Plans for FY11-13:

The objective for FY11-13 is to build on the operational experience with the LLD for long pulse experiments in NSTX. If the LLD provides the anticipated particle control, the fueling requirements for long pulse operation will be met with advanced capabilities such as pellet and compact toroid injection.

The LLD itself will be further upgraded for long pulse plasmas. The present LLD has been designed for particle pumping with static lithium surfaces; as such, it will have

limited heat removal capabilities. An upgrade to the LLD is envisioned during FY11-12, possibly consisting of a mesh-based system or technical improvements to the heaters, etc. Finally a long pulse divertor design will be needed around the time of the center stack and NBI upgrades. A flowing lithium system (LLD-Upgrade) is a candidate to handle the high heat fluxes and long pulses, depending on the success of the LLD. Experiments on CDX-U demonstrated that convection can play a major role in dissipating heat for liquid lithium²¹. By reducing the flow requirements for the liquid lithium, this has the potential of greatly simplifying the LLD-Upgrade design. IR cameras would be used to determine if convection is indeed occurring in such a system.

Fueling Plans for FY11-13:

While the near-term fueling plans focus on improvements and optimization of gas fueling, the longer-term goals are the implementation of a cryogenic pellet injector for central fueling, and a compact toroid injector for edge fueling and profile control. Pellets are a well-characterized core fueling option which would enable a range of additional studies, e.g. high density limits beyond Greenwald scaling, perturbative transport experiments, etc. The CT injector would provide not only efficient fueling, but also a possibility of ionization profile control and plasma profile control (including the momentum profile as the CT is a momentum source), both being attractive features for high-performance scenario optimization. Regarding this option, the CT injector previously used on the TdeV device is being stored on-site at PPPL. The cost of bringing the CT injector on-line would include retro-fitting it to NSTX and supporting a CT-centered fueling program. A programmatic decision on whether to install a pellet injector and/or the CT injector will be made in FY 2010, depending on the need for core fueling techniques with LLD operation. These tools would be available for the FY 2012 run.

Sec. 5.1.2 – SOL turbulence and width program

1. Introduction

The ‘scrape-off layer’ (SOL) is the region of the boundary plasma just outside the magnetic separatrix or last-closed-flux surface (LCFS). Most of the heat and the particle flux which exits from the main plasma enters the SOL and then flows along and across the magnetic field to the first wall or divertor plates. The width of the SOL is a measure of the radial distance over which the plasma parameters decay by $(1/e)$ outside the separatrix or LCFS. There are generally different widths for density λ_n , temperature λ_T , and total heat flux λ_q , and these can vary under different plasma conditions and at different places around the tokamak.

The importance of the SOL width is that it determines the local heat and particle fluxes to various parts of the wall and divertor. The local heat flux to the divertor plate must be kept below material damage limits, which becomes difficult to do if the heat SOL width is too small. Furthermore, the local particle flux must also be kept high enough to allow efficient exhaust of helium ash at the pumping port near the divertor plate. In addition, the heat and particle flux at other locations around the machine must also be low enough to avoid damage to those components, and the plasma density near some of the RF heating antennae must be high enough for good coupling. Besides these constraints on the SOL plasma itself, the SOL width may also indirectly affect several core plasma properties such as the impurity content, plasma rotation, and energy confinement. All of these interacting physics issues and potentially conflicting requirements make an understanding of the width of the SOL an interesting and important topic. The main proposed facility enhancements: 1) LLD, 2) larger center stack for higher I_p , B_t and longer pulse, and 3) second NBI system will enhance the research in this area by enabling a larger β range, lower v^* , and higher P_{SOL} , extending physics studies closer to the parameter ranges for next step STs.

2. Background and results

Measurements have been made of tokamak SOL parameters and widths for many years with consistent results, e.g. $\lambda_n \sim 1-3$ cm (see Ref. ²² for an early review, and Ref. ²³

for a recent review of JET results). These widths are the net result of the perpendicular transport across B over a timescale determined by the parallel transport to the divertor plates. Modern edge codes such as UEDGE²⁴ and B2-Eirene²⁵ still can not explain (or predict) these SOL widths from first principles due to an incomplete understanding of the physics that determines the perpendicular (and to some extent the parallel) transport. The goal of NSTX SOL research is help to provide such an understanding, from which it should eventually be possible to predict the SOL width in future tokamaks like ITER.

The parallel transport processes in the SOL are generally considered to be dominated by the classical heat and particle conduction along B. Recently NSTX has already made a significant contribution by testing this assumption experimentally. The upstream SOL widths for T_e and n_e as measured by the mid-plane fast reciprocating probe ($z = -18\text{cm}$) were compared with the target heat flux (q_{target}) width measured by IR camera. The use of an offset exponential for the profiles in the parallel conduction equation led to an additional factor to the theoretical relation between T_e and q_{target} SOL widths. The ratio of these two values showed an agreement between theory and experiment within $\sim 20\%$, implying that the parallel electron conduction for the near-SOL was consistent with the classical model²⁶.

The perpendicular transport in the SOL is generally considered to be dominated by turbulence, including both diffusive and convective (intermittent or ‘blob’ transport) processes. NSTX has also made significant contributions to the measurement and understanding of these transport mechanisms. The gas puff imaging diagnostic (GPI)²⁷ was developed at NSTX to measure SOL turbulence and was used to characterize the

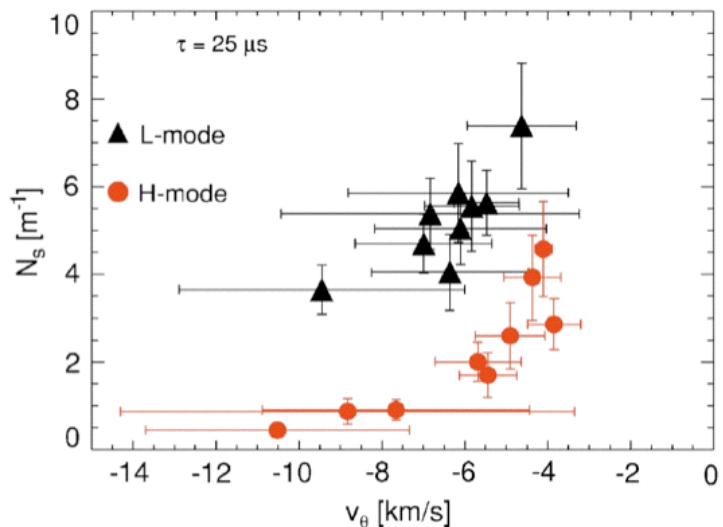


Fig. 5.1.2.1- Blob density vs/ poloidal propagation speed from GPI analysis.

structure of coherent filaments or ‘blobs’ in the SOL^{28, 29}; for example, the linear density of blobs was seen to decrease significantly from L-mode to H-mode, as shown in Fig. 5.1.2.1. SOL profiles and turbulence characteristics were measured using Langmuir probes³⁰ and compared with the results from DIII-D. In the area of theory, initial studies have been carried out by the Lodestar group^{31, 32}. It was found that the observed radial blob velocities in NSTX are bounded by theoretically predicted maximum and minimum velocities corresponding to the sheath-connected and resistive-ballooning regimes of blob transport (see Fig. 5.1.2.2)³³.

3. Empirical studies and exploration (FY09-10 and FY11-13)

Given our present limited theoretical understanding of the SOL width, it is useful to continue empirical studies and scalings^{34, 35}, and to explore new regimes and measurement techniques. In particular, empirical results on the comparison between carbon and lithium divertor surfaces will be a unique contribution from NSTX. These results will be especially valuable to help estimate SOL widths in future ST devices such as NHTX and ST-CTF.

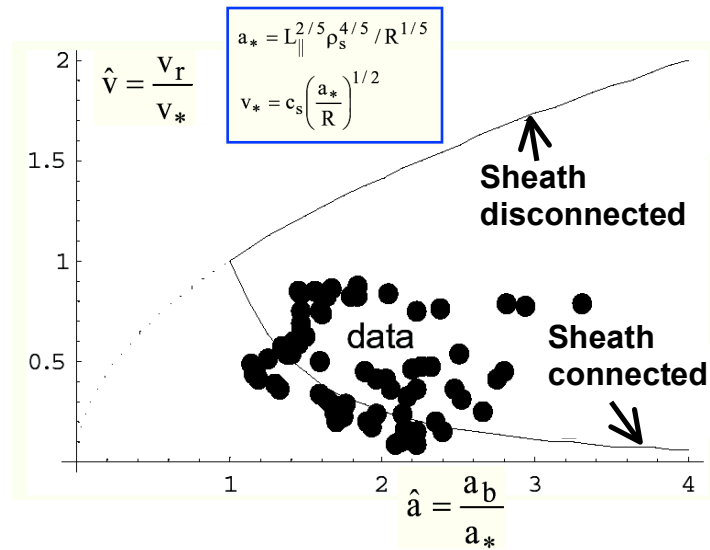


Fig. 5.1.2.2- Normalized blob speed vs. normalized blob radius from NSTX data.

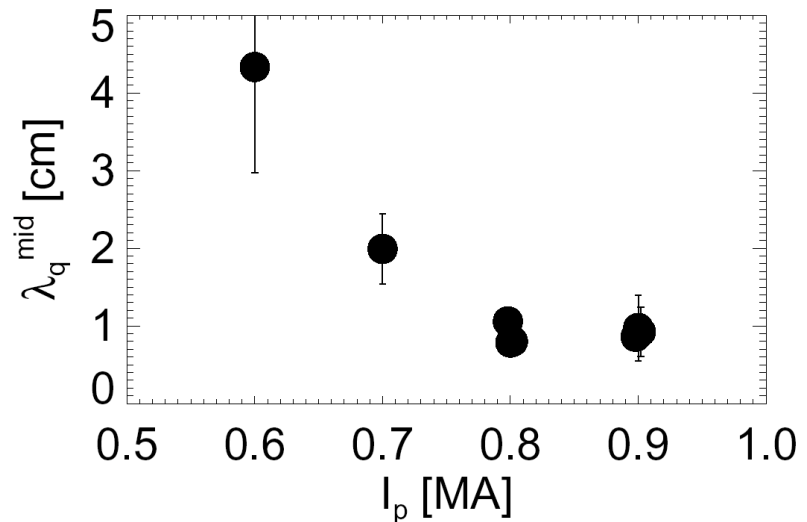


Fig. 5.1.2.3- Heat flux profile (λ_q^{mid}) width decreased with plasma current (I_p)

Plans for FY2009-2010:

a) study of SOL widths:

Variation of the target IR heat flux SOL width as well as the fast probe mid-plane SOL widths (T_e and n_e) as a function of plasma operation parameters will be experimentally investigated. Both the mid-plane and target profiles became narrower in the near SOL with increasing plasma current (Fig. 5.1.2.3) and experiments should be conducted to reveal the dependence on I_p , \bar{n}_e , and input power in more detail. The SOL width data will be scaled with plasma operation parameters and the scaling law will be compared with analytical models. The simultaneous measurement of the SOL widths and blob characteristics will also allow a study of the link between the two. The LLD will enable access to lower v^* , closer to that envisioned for next step STs.

b) study of edge turbulence:

We plan to continue measurements of edge turbulence utilizing the existing GPI and Langmuir probe hardware to extend previous experience and results. We will study the process of the generation of intermittent filaments (blobs) from edge turbulence and the radial transport of the filaments in the midplane SOL, which very likely affects the SOL widths. We will also make new GPI measurements of the turbulence and filaments in the divertor region (including the private flux region), which may affect SOL of heat/particle flux at the divertor plate itself, and will measure the correlation between the midplane and divertor filament structures, such as shown in Fig. 5.1.2.4. All of these measurements will contribute to testing specific theoretical models for the SOL (see Sec. 4). An important upgrade of the NSTX Langmuir probe system to measure T_e fluctuations is planned.

Plans for FY2011-2013:

a) An additional reciprocating Langmuir probe located near the X-point would add an extremely valuable diagnostic capability to the study of the SOL width of NSTX. Specifically, this X-point probe would be useful to look at poloidal symmetries, X-point

physics (e.g. the resistive X-point instability), ELM dynamics and parallel heat transport issues.

b) The present NSTX GPI diagnostic utilizes two state-of-the-art fast framing digital cameras fielded by Nova Photonics Inc. These cameras, each capable of running at ~ 120000 frames/s and with frame synchronization between the two cameras to within

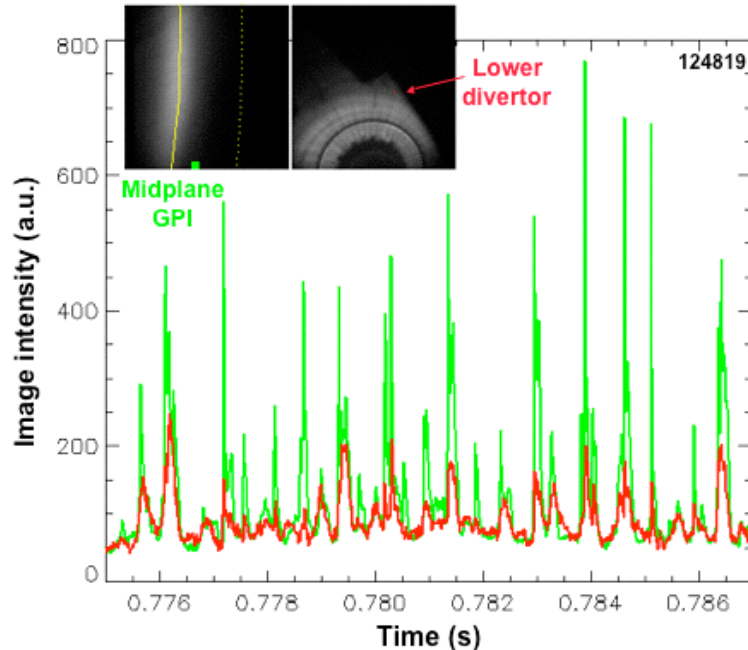


Fig. 5.1.2.4- Midplane GPI peaks (green) correlate in time with divertor GPI peaks (red).

0.25 ms, can image small sections of the plasma edge with high spatial resolution, thus providing unequal physics data well suited for the research indicated above. This capability will be improved during the period 2011-12 as the imaging technology is developed, thus providing further improvements in the diagnostic capabilities.

4. Testing specific theoretical models (FY09-13)

At the present time the fundamental physics determining the SOL width and profiles is not well understood. In the next few years we will use NSTX data to test specific theoretical models and simulations to validate these models so that an eventual understanding of this physics can be obtained.

Plans for FY2009-2010:

a) The Lodestar group plans to carry out detailed validation/comparison studies between its newly developed SOLT (Scrape-Off-Layer Turbulence) code and the NSTX GPI and Langmuir probe data. NSTX will collaborate with the Lodestar group on these blob model validation studies to understand blob formation and intermittent transport; for example, a simulated GPI diagnostic capability has been added to SOLT in collaboration

with PPPL staff. In addition, the NSTX/Lodestar collaboration has proposed experimental tests to address (i) blob speed in disconnected/detached plasmas, (ii) parallel blob-filament structure in the presence of X-points, (iii) ICRF interaction with edge turbulence (see also Sec. 5).

b) The LLNL group is planning to conduct a systematic analysis of turbulence and transport in the SOL using both analytic models and the BOUT code, and to compare these results with NSTX data. In the BOUT model, the fluid turbulence determines the radial flux of particles and heat, and parallel fluid transport determines the average axisymmetric profiles. Due to the time scale separation between turbulence and transport it may not be practical to calculate self-consistent SOL profiles within a turbulence model. To overcome this difficulty one may resort to the projection-integration method developed for this class of problems³⁶. This approach has been used, with coupling the turbulence code BOUT and edge transport code UEDGE. Some results with self-consistent edge were obtained^{37, 38}, however for a more comprehensive study we are planning to revisit it in the near future.

c) The CPES group plans to use the XGC0 kinetic particle code to simulate the SOL plasma in NSTX, including the magnetic separatrix, X-point and material wall³⁹. There will be a specified heat flux from the core plasma and particle source from neutral ionization, and the self-consistent radial electric will be evaluated. The only free parameter in the present model is the anomalous radial diffusion rate. We will study the sensitivity of the calculated scrape-off layer width to the wide range of pedestal plasma profiles, neutral recycling positions and rates, and assumed anomalous diffusion rates, and compare the results with experimentally measured heat deposition profiles on the divertor target plates of NSTX. Later versions of the code will include an edge turbulence model to calculate the SOL widths and profiles self-consistently.

Plans for FY2011-2013:

Each of these modeling and validation projects should be continued as the codes are developing and further validation experiments become feasible. This process can potentially continue using archived NSTX data if NSTX does not operate during this

period.

5. Methods to control the SOL (FY09-10 and FY11-13)

Even if a predictive theoretical understanding of the SOL width can be achieved, it is possible that the resulting widths will not be consistent with successful operation of future high powered tokamak devices such as ITER or NHTX. Therefore we need to develop methods to actively control these SOL widths, e.g. to increase them to reduce the peak heat flux at the divertor plate. These potential control methods can also be simulated using the models discussed in Sec. 4, and so provide interesting tests of these models.

Plans for FY2009-2010:

a) ‘blob’ detachment: Plasma detachment normally decreases the heat flux to the divertor by increasing the radiated power in the edge. The Lodestar group has proposed that the SOL width can also be increased by detaching these filaments from electrical contact with the divertor sheath using gas puffing in the divertor region, which will cause an increase in the filament’s ExB radial drift velocity. Initial tests of this idea will be made by measuring the radial filament speed with and without detachment using the GPI midplane and divertor systems.

b) convective cell generation: The LLNL group has proposed that the SOL can be increased by non-axisymmetric electrical biasing of the divertor plates to create small-scale convective cells⁴⁰. Successful experimental tests of this idea have been made using a set of biased electrodes near the outer midplane of NSTX⁴¹. These experiments will be extended in FY2009-2010 to include biasing small electrodes mounted in divertor plate tiles between the LLD segments. The Lodestar group has also proposed that convective cells can be generated by RF sheaths and used to spread the heat load in the divertor⁴², and initial tests of this idea will be made using the HHFW antennas in NSTX.

Plans for FY2011-2013:

The SOL control methods described above do not require any significant hardware modifications to NSTX. Given additional time, we could potentially test

additional ideas that will require a significant modification to NSTX hardware. For example, if the small divertor tile biasing experiments in NSTX are successful in FY2009-2010, a system for larger-scale biasing of the divertor plates for SOL control might be installed and tested during FY2011-2013.

5.1.3 ST divertor physics and heat flux control

1. Introduction

Steady-state mitigation of divertor heat flux and material erosion are critical issues for both the International Thermonuclear Experimental Reactor (ITER) and especially spherical torus (ST) based devices, which are designed to be high power density systems. Owing to their compact nature, spherical tori (ST) have the potential for high heat flux at divertor target plates because of the large ratio of P/R , where P is the heating power and R is the major radius of the device. One example: a Component Test Facility (CTF) design⁴³ based on the ST concept has a P/R of about 35, above the value for ITER, and it requires an 85% radiated power fraction to maintain target peak heat flux below 15 MW/m². Furthermore, the combination of the high edge magnetic field line pitch, the short connection length, the high magnetic mirror ratio in certain configurations, and relatively low B_t can lead to a rather different divertor physics operational regime in NSTX.

At present, candidate heat flux mitigation techniques include use of radiative/detached divertors and/or divertor geometry optimization, including the deployment of novel divertors. Looking forward, heat flux control must be demonstrated in low-density Li-pumped discharges. The ultimate goal is to develop an experiment-based predictive capability of heat flux distribution and control for the next-step ST-based fusion devices.

2. Background and results

In an ST magnetic geometry, access to the radiative divertor as well as its efficiency was predicted to be difficult because of the large P/R , and because of geometric features of the ST divertor - a small plasma volume, a small plasma-wetted area, a short parallel connection length, and a large inboard to outboard plasma surface asymmetry, as shown in Table 1. The ST effects, most notably, the geometric SOL structure, lead to observed differences in NSTX divertor operating regimes. Recent NSTX experiments have demonstrated both similarities and differences in the divertor regimes observed in NBI-

heated plasmas, as compared to conventional tokamak results. Divertor regimes have been characterized for both low κ , δ and high κ , δ configurations.

Table 1: comparison of geometric characteristics of NSTX and high aspect ratio tokamak, e.g. DIII-D

Quantity	NSTX low $\kappa \sim 2, \delta \sim 0.5$	NSTX high $\kappa \sim 2.3, \delta \sim 0.8$	Tokamak
Aspect ratio	1.3-1.4	1.4-1.5	2.7
In-out SOL area ratio	1:3	1:3	2:3
Midplane to target connection length L_c (m)	10-12	8-10	30-80
X-point to target parallel length L_x (m)	6-8	5-7	10-20
X-point to target poloidal length L_p (m)	0.15-0.25	0.05-0.15	0.05-0.25
Poloidal magnetic flux expansion f_m at OSP	3-4	16-24	3-15
Field angle at target (degree)	5-15	5-15	1-2

In NSTX, the typical H-mode operating scenario leads to a well-attached outer divertor leg with high peak heat flux, and a detached inner divertor leg with rather low heat flux⁴⁴. The first detailed study on the dependence of outer divertor peak heat flux in H-mode on two key parameters, P_{NBI} and I_p , has been published, building on an earlier study of L-mode plasmas⁴⁵. This study demonstrated that the peak heat flux increased monotonically with the power flowing in to the SOL (P_{LOSS}), with a break in the slope

between 2 and 3 MW (Figure 5.1.3.1)⁴⁶. To obtain insight into the experimental trends, these data were simulated with a two-point model of the SOL derived by K. Borass⁴⁷. These simulations suggested that the break in the slope corresponded to a transition from a near detached regime through the high recycling regime (see Figure 10 blue, green, and red curves and the publication for details⁴⁶).

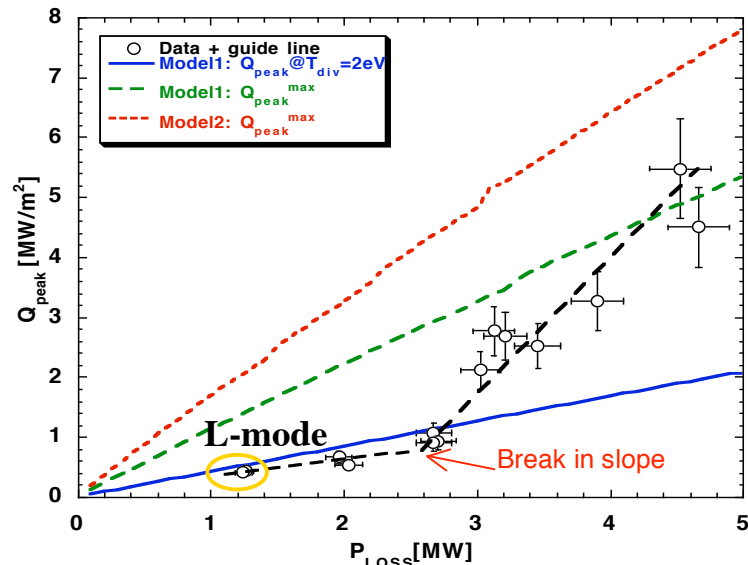


Fig. 5.1.3.1- Dependence of outer divertor peak heat flux (Q_{peak}) on SOL loss power (P_{LOSS}), and comparisons with Borass' 2-point model calculations of the NSTX SOL.

Even higher heat fluxes, up to 10 MW/m^2 , have been measured in lower density plasmas^{48, 49}. The peak heat flux was also shown to increase rapidly with I_p , with a much stronger dependence than a simple connection length dependence observed in two-point models; the profile width also shrunk with I_p . Power accounting was not very good, i.e. up to 70 % of P_{in} could be accounted, with up to 10 % divertor radiation even at the highest densities⁵⁰.

Several different techniques to mitigate the peak heat flux have been used. The simplest technique is by control of the boundary shape: it was shown that the peak flux was decreased by about 50% in comparing a LSN to a DN with otherwise similar shape parameters, and reduced again by 60% in comparing the standard DN to a high δ DN with substantially increased flux expansion⁵¹ (Figure 5.1.3.2). In that particular study, we note that the heat flux profile was rather broad, suggesting that partial detachment and radiation may have contributed to the heat flux reduction.

Dedicated radiative and detached divertor scenarios has also been investigated, the latter being differentiated by signs of volume recombination⁵²⁻⁵⁴. In low δ , lower-single

null discharges, partial divertor detachment (PDD) and heat flux reduction by 60-80% was achieved. However, the PPD regime could be obtained only with high D_2 injection rates that led to an X-point MARFE formation and confinement degradation. The limited access to detachment was found to be qualitatively consistent with predictions of zero- dimensional two point models and two-dimensional multi-fluid modeling with the

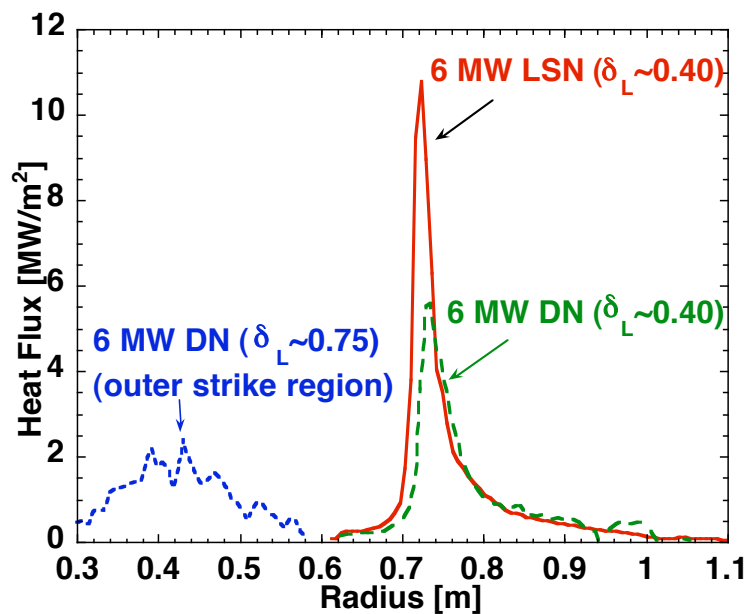


Fig. 5.1.3.2- Peak heat flux is reduced comparing in $\delta \sim 0.45$ single-null (red) and double-null (green). It can be reduced further at high $\delta \sim 0.8$ (blue), owing to higher flux expansion and relatively easier access to partial detachment.

b2.5 and UEDGE codes. The main conclusion was that it was difficult to maintain the adequate steady-state volumetric power and momentum losses required for detachment at high parallel heat flux $q_k=30\text{-}50\text{ MW/m}^2$ in the open geometry carbon divertor with a short parallel length and poor gas entrapment, typical of the lower-end κ,δ configurations.

More promising results were obtained in high δ , lower-single null discharges, in that similar levels of heat flux control were achieved without degradation of the energy confinement. These baseline discharges showed improved plasma performance approaching the performance level of CTF with high $\beta_t = 15\text{-}25\%$, high $\beta_N = 5.7$, and a high bootstrap current fraction $f_{BS} = 45\text{-}50\%$ sustained for several current redistribution times. Higher plasma shaping factor also led to longer plasma pulses, and an H-mode regime with smaller ELMs, long with heat flux naturally reduced by 30-50 % because of higher flux expansion.

This high flux expansion divertor configuration has geometric properties facilitating access to detachment, because of a higher radiative volume, and a possible plasma "plugging" effect counterbalancing the openness of the NSTX divertor⁵⁴. The PDD regime was obtained in NSTX in this configuration at several SOL power levels, corresponding to the highest q_{peak} values achieved with 4-6 MW NBI input power, and $I_p = 0.8 - 1.0\text{ MA}$ (Figure

5.1.3.3). The core stored energy and confinement time were practically unaffected. Divertor power and momentum losses measured in the PDD phase indicated similar trends with large aspect ratio tokamak experiments, e.g. a 30-60 % increase in divertor plasma radiation, a significant increase in neutral pressure

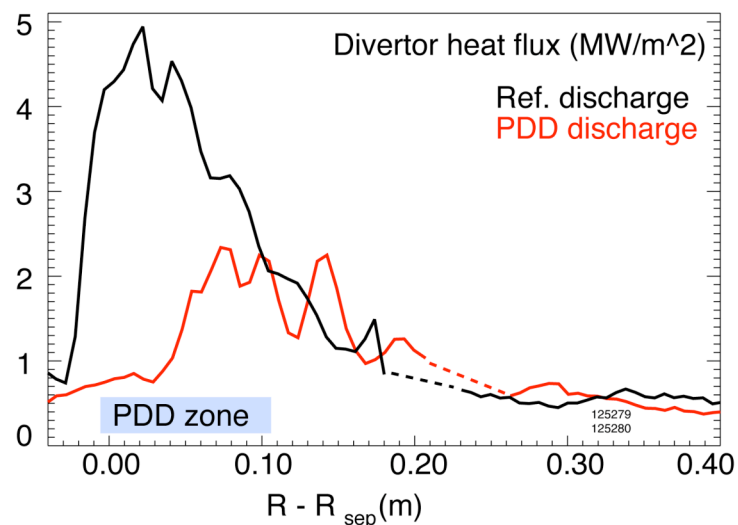


Fig. 5.1.3.3- Comparison of heat flux profiles in reference and partially detached (PDD) discharge in high $\delta \sim 0.8$ configuration.

and recombination rate, and the peak heat flux reduction up to 60 %, measured in a ~ 0.1 m radial zone. An analytic 1D five-region SOL transport model⁵⁵ with constant heat and particle sources and sinks predicted that large radiated power and/or momentum loss fractions were required to achieve detachment in the NSTX range of parallel SOL heat flux $q_{\parallel} = 25\text{-}60 \text{ MW/m}^2$ and connection lengths $l_{\parallel} = 6\text{-}10 \text{ m}$ ⁵⁴. This model is shown schematically in Fig. 5.1.3.4, along with the predicted n_e and T_e variation along field lines in the SOL in the high recycling and detached scenarios. In agreement with experiment, the model predicted that it was nearly impossible to reach the detachment by simply increasing plasma density in NSTX. However, increasing the fraction of neutral re-ionization in divertor by 50-90 %, thereby simulating a divertor gas injection, lead to a relaxation of the divertor radiated power fraction requirement to realistic P_{rad} levels (40-60 % of P_{in}). An assessment of intrinsic carbon divertor radiation using a 1D SOL heat conduction model with

non-coronal carbon radiation indicated that it was marginally possible to reduce the parallel heat flux to low levels with realistic divertor carbon concentrations ($c_{carbon} < 10 \%$). Thus, combined divertor geometry effects appeared to play

a favorable role in promoting detachment in the high flux expansion open divertor configuration, showing much promise for future ST radiative divertor and novel high flux expansion divertor applications.

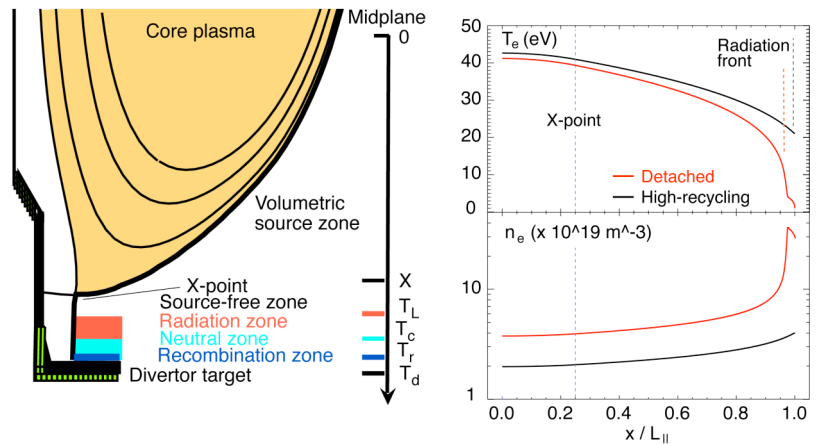


Fig. 5.1.3.4- 5-zone interpretive model showing variation of n_e and T_e along the field line for NSTX high recycling and detached cases.

3. Plans

The goals for the next five-year period in the scrape-off layer and divertor research area on NSTX are three-fold. The near-term research (FY09-FY11) will focus on general

heat and particle transport studies in the ST, including the effect of liquid lithium divertor on edge plasma properties. In later years (FY12-FY13), we plan to enhance these studies with advanced diagnostics and analysis, and design a new divertor capable of handling the higher I_p , B_t , and longer pulse length plasmas that will be enabled with the new center stack and solenoid. The new divertor would include advanced particle and power handling features, such as an upgraded liquid lithium module, new PFC target materials, a cryo-pump, and/or novel geometry (e.g., a “snowflake” divertor or an X-divertor).

Plans (FY09-11):

ST SOL and divertor studies

The goal will be to characterize SOL and divertor heat and particle transport, improving our understanding of the ST impurity effects. This research will contribute to the general tokamak SOL and divertor studies, and improve experiment-based projections toward the future ST-based fusion devices. An increasingly important aspect of this work will be the coordinated efforts and collaboration with Alcator C-Mod and DIII-D scientists. This would help to separate the ST-specific magnetic geometry effects from the configuration-specific effects.

The following research efforts are planned for this period:

- A. Comparison of heat flux profiles and plasma parameters at the divertor and outer midplane with models to identify the thermal transport processes in the SOL
- B. Transient (ELM-induced) divertor heat and particle flux studies, including: 1) the interaction of ELMs with a detached or radiative divertor scenario; 2) parallel transport of ELMs on the open field lines; and 3) the 3-D structure of the ELMs
- C. Private-flux region characterization and transport studies
- D. Lower divertor power accountability and MARFE characterization studies with new diagnostics

These new diagnostics commissioned during this period will provide essential data for these studies:

- New IR cameras, including a fast IR camera for transient event analysis, and the use of two-color techniques, for divertor heat flux profile measurements
- New divertor bolometer system: 16 channels to reconstruct the 2-D radiated

- power profile
- Ion flow measurement of the edge and SOL flow
 - An X-point reciprocating Langmuir probe for local n_e , T_e and fluctuations
 - Imaging divertor UV-VIS spectrometer for divertor T_i , impurity radiation, divertor n_e and T_e profiles
 - New “smart” tiles as part of the LLD program between LLD segments, with a dense Langmuir probe arrays, and thermo-couples, for divertor particle, heat flux, n_e and T_e profile measurements.

Data analysis and interpretation will include the application of 2D multi-fluid (UEDGE²⁴, SOLPS²⁵) and neutral (DEGAS-2⁵⁶) numerical models, as well as reduced-dimension (2-point, 1D, onion-skin) models⁵⁷.

Divertor properties with LLD (also summarized in section 5.1.1 plans)

As the LLD research is an important part of the NSTX program in FY09-FY11, the boundary physics effort will provide a comprehensive LLD characterization and cover dedicated experiments to clarify the impact of the LLD on edge plasma characteristics. The goal is to document the LLD module performance under various plasma conditions, and to investigate the pumping and heat flux handling capabilities of the LLD. The following topics will be addressed:

- A. LLD pumping characterization
- B. Divertor operating regimes with lithium pumping and strong lithium radiation, as functions of input power, density, impurity density
- C. Divertor heat flux handling, detachment operating space, and comparison of detachment and X-point MARFE onset with data from tokamak experiments
- D. Impurity sources, i.e., chemical and physical sputtering, in the presence of mixed target materials
- E. Role of molecular fluxes, since a number of D-, B- and Li- containing radicals are formed in the low temperature PFR plasmas

These studies will utilize a number of existing and newly commissioned diagnostics:

- New IR cameras, including a fast IR camera, and ones using two-color techniques, for divertor heat flux profile measurements

- New divertor bolometer system
- New Lyman- α diode arrays, to replace existing visible Balmer- α and Balmer- β arrays, rendered inadequate in the presence of highly reflective lithium coatings
- Imaging divertor UV-VIS spectrometer, to provide divertor ion temperature, impurity, divertor n_e and T_e profiles
- New “smart” tiles, being a part of the LLD module design, will include dense Langmuir probe arrays, and thermo-couples, for divertor particle, heat flux, n_e and T_e profile measurements.

Data analysis and interpretation will include the application of codes mentioned above, as well as atomic data from ADAS database and collisional-radiative modeling. The emphasis will be on developing a comprehensive model of plasma-LLD interaction, which will utilize plasma and Monte Carlo neutral transport models, and the TRIM code and molecular dynamics calculations for plasma-lithium surface interaction.

Divertor heat flux mitigation studies

The heat flux control effort will continue to provide important answers for projections to the upgraded NSTX and future ST-based devices. In FY09-FY11, the emphasis will be on experimental studies of heat flux mitigation solutions with existing facility capabilities. The following research efforts are planned in this period:

- A. Optimization and control of partially detached divertor regime with impurity and deuterium injection at high input power and reduced density, integration with long-pulse H-mode scenarios, and in double-null configurations
- B. The use of resonant magnetic perturbations to split/sweep the strike point and reduce peak heat flux
- C. Development of heat flux mitigation solutions with novel flux expansion configurations with existing magnetic coils, e.g., the “snowflake” divertor⁵⁸. While a pure snowflake divertor is thought to be topologically unstable, modest coil current variations can be used to create stable equilibria with high flux expansion. Preliminary calculations have suggested that a ‘snowflake-plus’ geometry can be achieved in NSTX with the existing coil set (Figure 5.1.3.5).

Plans (FY12-13)

Between FY11 and FY 12, the center stack and central solenoid will be replaced in NSTX, with the goal of achieving 2 MA, 1 T discharges with pulse length up to 5sec. For NSTX ATJ divertor graphite tiles, a peak heat flux of $\sim 6.5 \text{ MW/m}^2$ would result in exceeding the $1200 \text{ }^\circ\text{C}$ administrative limit at the end of the 5 sec pulse. Peak heat fluxes of this magnitude are routinely encountered in LSN discharges with $P_{\text{NBI}}=6 \text{ MW}$. Moreover the use of Li (leading to ELM-free discharges) tends to reduce the SOL heat flux width by up to 50%, resulting in up to a 100% increase in peak heat flux. Thus a combination of heat flux mitigation schemes could well be required for this operation, including the use of DN geometry with high flux expansion, radiative/detached divertors (if compatible with low collisionality operation), and new divertor schemes. This need will be amplified with addition of the second NBI, the preparation for which is in FY112-13, and implementation would be FY 14.

In anticipation of these long pulse upgrades, a divertor geometry upgrade is planned, the precise details of which will be worked out over FY09-10. The likely candidate is installation of extra PF coils to create the X-divertor, or perhaps even multiple coils which would allow a Super X divertor geometry (Figure 5.1.3.6). In short, the X-divertor increases the poloidal flux

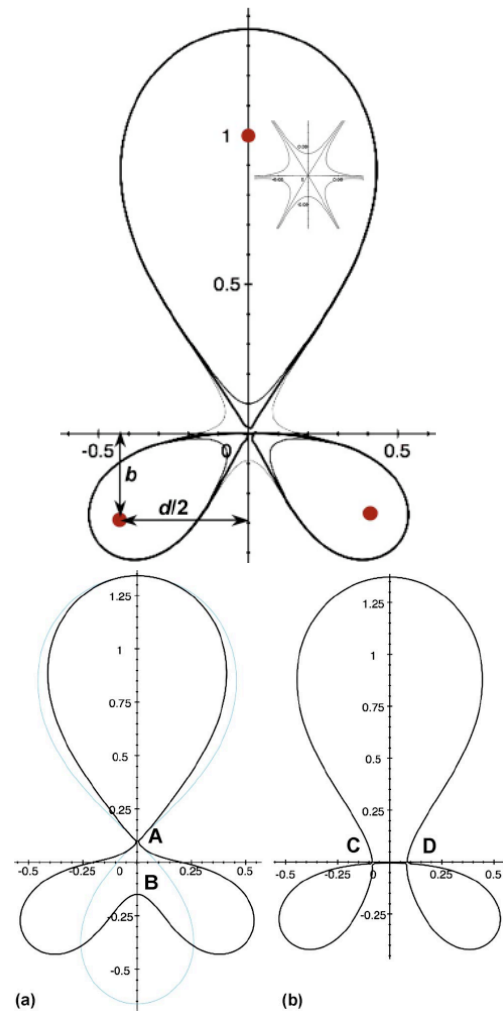


Fig. 5.1.3.5- Plot of separatrix in a snowflake divertor from ref. 58. Panels (a) and (b) represent $\pm 5\%$ changes to coil currents to create a 'snowflake-plus' and a 'snowflake-minus', each of which have higher flux expansion than a standard X-point divertor.

expansion by adding a secondary X-point just outside the primary one, whereas the Super X-divertor also moves the outer strike point to large major radius to increase the plasma wetted area and the field line connection length/radiation volume. The Super-X divertor would also require modification of the secondary passive stabilizing plates and installation of a target near the vacuum vessel wall. It could be made compatible with Lithium coatings and/or a local cryopump for improved pumping.

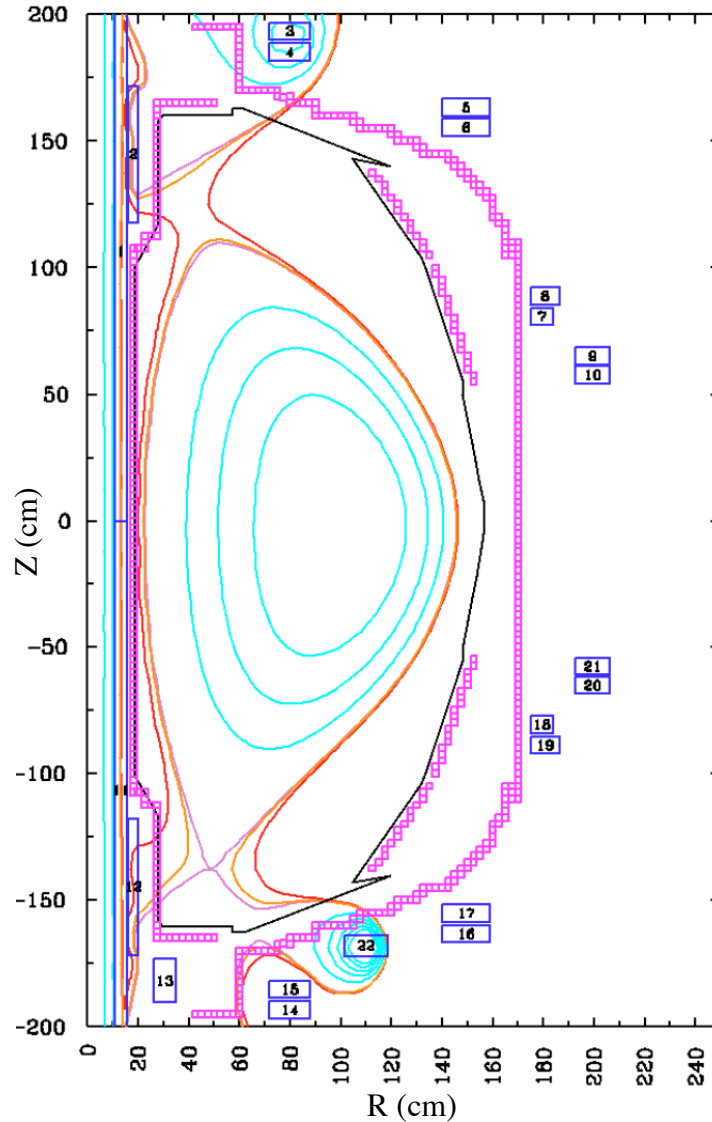


Fig. 5.1.3.6- Preliminary calculation of super-X divertor geometry possible with the addition of a single coil (#22) between PF2 (14, 15) and PF3 (16,17). Optimization of the geometry is in progress. Courtesy of P. Valanju, M. Kotschenreuther, and S. Mahajan (UT-Austin).

5.2.1 H-mode pedestal and ELM physics

1. Introduction

The correlation between performance of the plasma core and the plasma temperature at the top of the H-mode pedestal has been established in tokamak experiments from the past decade. Studies examining many devices have shown^{59, 60} that the highest pedestal temperature occurs at low pedestal collisionality, a region that is typically accompanied by large edge-localized modes (ELMs). Large or Type I ELMs result in a periodic exhaust of a substantial portion of the plasma stored energy to the plasma-facing components (PFCs). Localized melting of the PFCs would occur in the International Thermonuclear Experimental Reactor (ITER) if the ELM energy deposition were to exceed the PFC heat handling capability, which would effectively impose a limit on the ITER PFC lifetime⁶¹. Fig. 5.2.1.1 shows one multi-machine database of Type I ELM size vs. the parallel flow time in the SOL, thought to be one of the important physics parameter for

extrapolation. By this measure, estimation of ITER's ELM size is an interpolation within the existing data set, with a predicted pedestal fractional stored energy loss of about

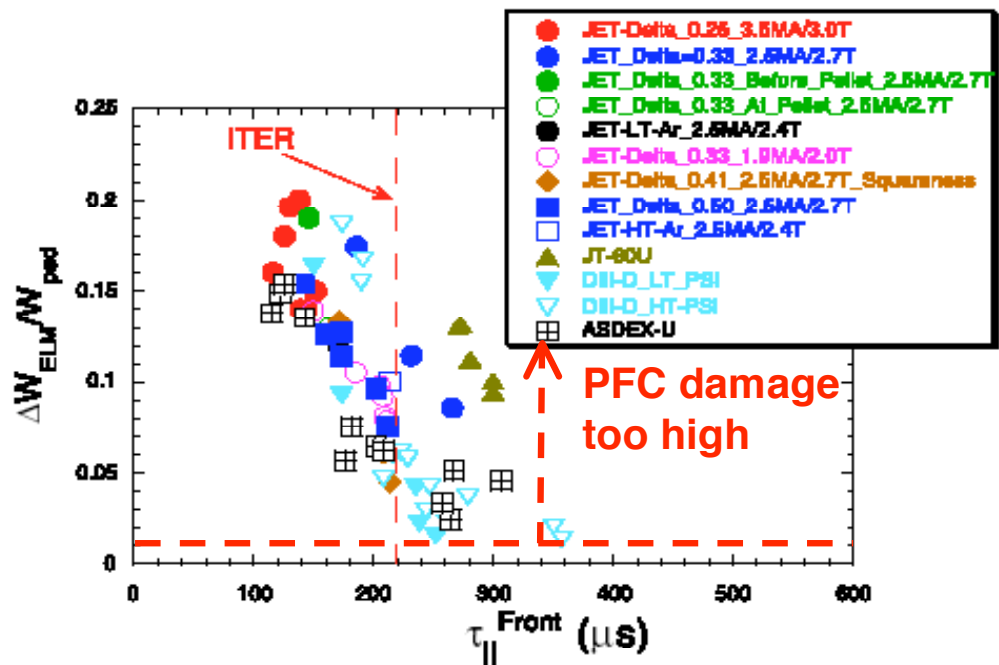


Fig. 5.2.1.1- International database of fraction pedestal energy loss per Type I ELM as a function of a parallel flow time from ref. 60. The ITER specification on $\Delta W_{ELM}/W_{ped}$ was revised downward to 1%, i.e. Type 1 ELMs are unacceptable.

4%. This value compares with an acceptable pedestal stored energy loss per ELM of 1%. Other extrapolation models and scalings are less favorable, with the conclusion that repetitive Type I ELMs are unacceptable in ITER.

Accordingly the quest for high confinement regimes with no or small ELMs has received increasing priority in the fusion research community. Several promising regimes have been identified which maintain the H-mode transport barrier: small, Type II ELMs from shaping⁶²⁻⁶⁴ or high density operation^{65, 66}; grassy ELMs⁶⁷; the Enhanced D_α H-mode⁶⁸ and High Recycling Steady H-mode⁶⁹; the Quiescent H-mode⁷⁰; and the suppression of large ELMs with externally imposed edge resonant magnetic perturbations⁷¹. While the last one is the preferred ITER method for ELM suppression, many outstanding issues exist concerning the design of ELM control coils and the extrapolability of successful results from present day machines.

The H-mode pedestal is the region connecting the core plasma and the edge steep gradient and SOL plasma. A wide body of research has demonstrated the strong link between the core confinement and the H-mode pedestal parameters, owing to the existence of stiff transport. Thus an accurate prediction of H-mode pedestal parameters is integral for extrapolation to next step devices. In the simplest terms, the pedestal density, temperature, and pressure are represented as the product of a gradient and a width. In this manner, H-mode pedestal and ELM research is intricately linked because ELMS effectively set a limit to the edge pedestal pressure gradient. Substantial progress has been made on the identification of peeling and ballooning modes as the underlying instability responsible for large, Type I ELMs⁷². The physics responsible for setting the pedestal widths is not as well understood; as such a predictive model of the pedestal heights, as the product of width and gradient, requires further dedicated research. NSTX provides an important test-bed for such pedestal and ELM theories because aspect ratio is a leading order term in the stability calculations. Therefore, NSTX is actively participating in several pedestal/ELM related experiments sponsored by the International Tokamak Physics Activity (ITPA).

2. Background and results

ELM control research is an important element of the NSTX physics program, owing partly to the needs of long pulse operation and partly to the significance for ITER described above. Spherical tori such as NSTX have limited space for an ohmic transformer, leading to lower volt-second capabilities than higher aspect ratio tokamaks. Large ELMs can consume substantial flux in NSTX, leading to reduced pulse length⁷³.

A wide variety of ELMs has been observed^{74, 75} in NSTX, enabling a broad ELM research program and a straightforward connection to the studies from high aspect tokamaks. **Figure 5.2.1.2** shows several ELM types in NSTX: a large Type I ELM in panel (a), a medium-sized Type III ELM in panel (b), a small ELM discovered in NSTX

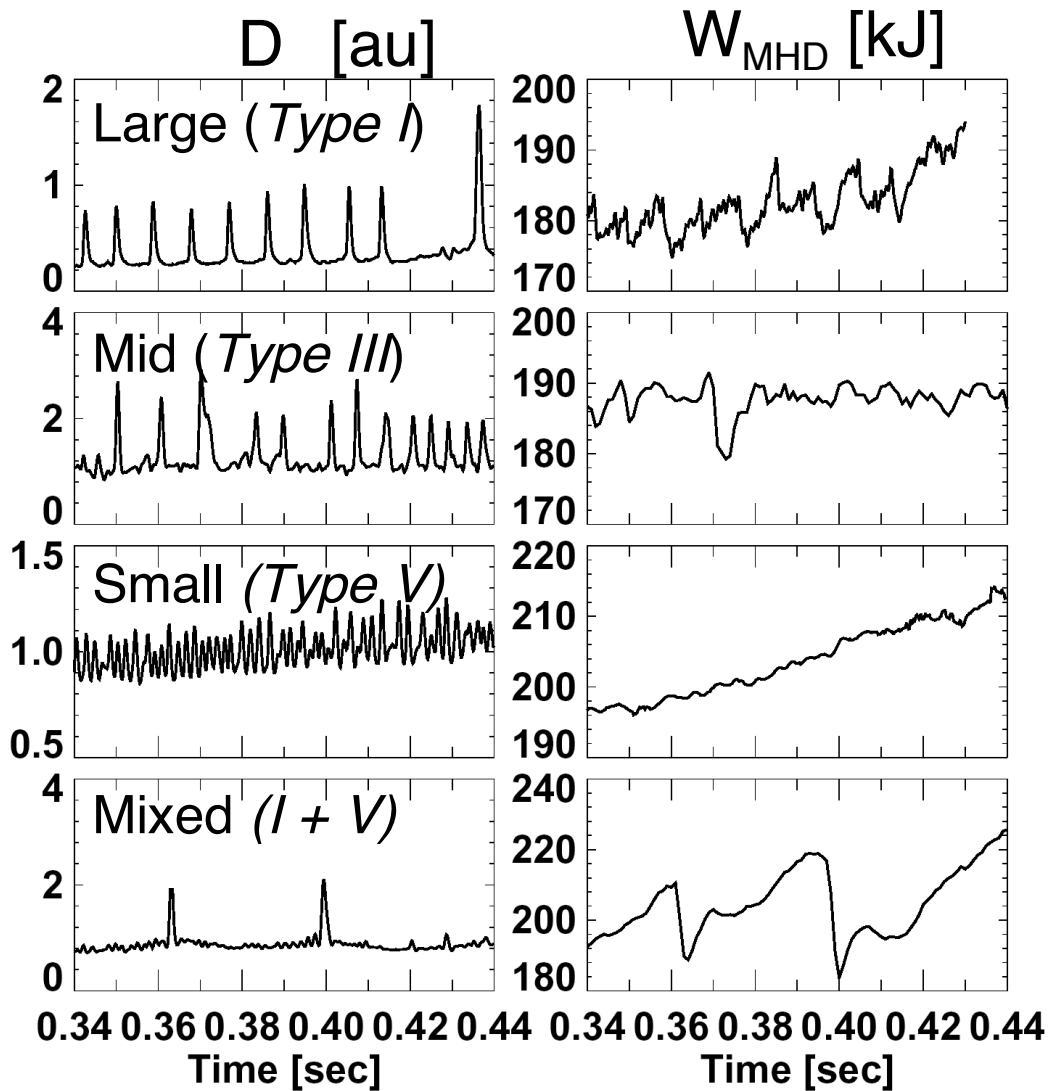


Fig. 5.2.1.2- Signature of different ELM regimes in NSTX, in divertor D_α emission and stored energy drop. At the highest heating powers, a mixed Type I + V regime is encountered.

and labeled as Type V in panel (c), and a “mixed” regime with both Type I and Type V ELMs in panel (d)⁷⁵. One measure of ELM severity is the reduction of the core plasma stored energy caused by the ELM. By this measure, Type I, III, and V ELMs typically result in a stored energy reduction of 3-15%, 1-5%, and $\leq 1\%$ respectively, although reductions as high as 30% are occasionally observed for the largest Type I ELMs.

Because of the broad interest in small ELM regimes, studies of the small, Type V ELMs have received high priority^{73, 76}. The main features of Type V ELMs are: 1) stored energy drop $\leq 1\%$ per ELM, 2) $n=1$ or $n=2$ magnetic signature, propagating counter to I_p and NBI direction, 3)



Fig. 5.2.1.3- filamentary structure of Type V ELM on wide angle camera.

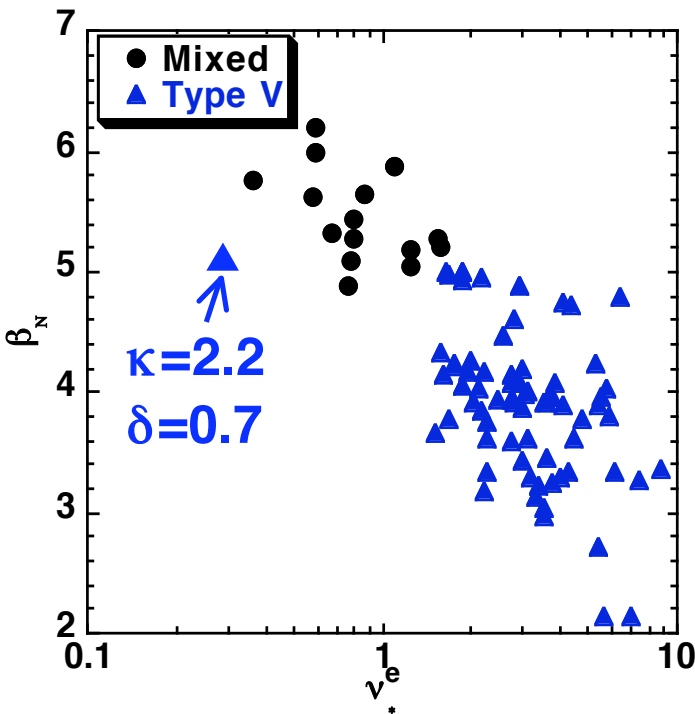


Fig. 5.2.1.4- Onset of mixed Type I + V ELM regime in normalized β and edge collisionality space for $\kappa=2$, $\delta=.45$. The onset point is moved to lower collisionality with more shaping, i.e. $\kappa =2.2$, $\delta =.75$.

characteristic single or double filamentary structure on various diagnostics (e.g. the visible camera image shown⁷⁵ in Figure 5.2.1.3), 4) existence only in plasmas with a dominant lower X-point, and 5) no poloidal beta threshold and no quasi-coherent edge MHD activity. At the upper end of the heating power available in NSTX, however, Type V ELMs appear inadequate for achievement of quasi-steady profiles, and thus Type I ELMs appear. The actual electron

collisionality ν_*^e at the time of Type I ELM onset depends on the plasma boundary shape⁷⁵ (Figure 5.2.1.4).

Community-wide tokamak research over the past five years has connected the onset of ideal MHD instabilities with the occurrence of large, Type I ELMs. Specifically, the edge plasma normalized pressure gradient in DIII-D was shown to be unstable to intermediate-n peeling or ballooning modes just before the onset of a Type I ELM⁷⁷. A similar calculation was used to predict that the pressure gradient limit should increase rapidly with inverse aspect ratio⁷⁸ (Figure 5.2.1.5). That study motivated an ITPA-sponsored experiment between NSTX, DIII-D and MAST to test the effect of aspect ratio on H-

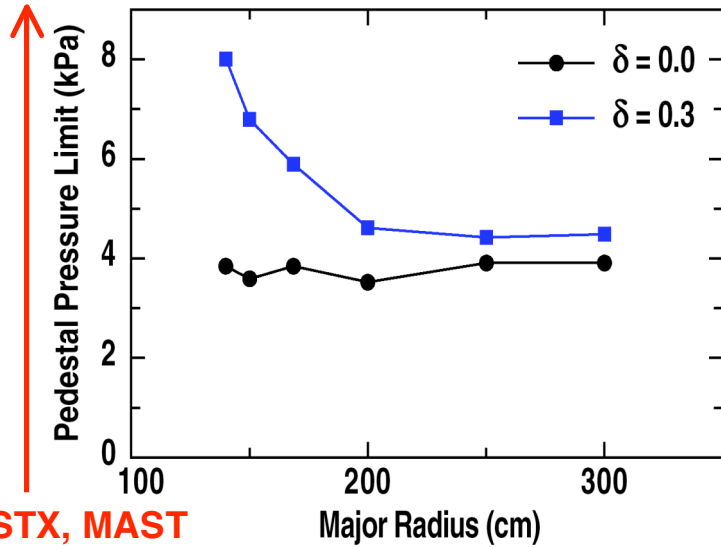


Fig. 5.2.1.5- Predicted pedestal pressure limit as a function of major radius at constant pedestal width, minor radius, I_p , and B_t , starting from a DIII-D equilibrium ($R=167$ cm). The major radii of NSTX and MAST are 85cm.

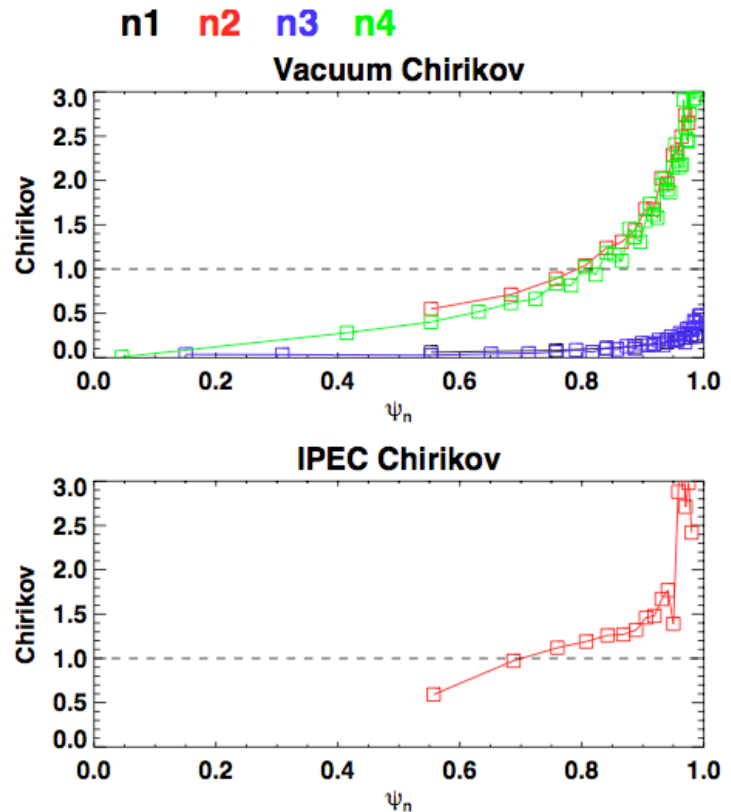


Fig. 5.2.1.6- Vacuum and IPEC-computed (i.e. including plasma response) Chirikov parameters for n=2+4 configuration.

mode pedestal heights, widths, and gradients. A common boundary shape was achieved⁷⁹ in all three devices while matching the pedestal normalized gyro-radius (ρ^*) and v_*^e , and all three devices exhibited Type I ELMs. Stability analysis showed that the DIII-D and MAST discharges were at either the peeling or ballooning stability boundary, whereas the NSTX discharges were computed to be stable.

While characterization of ELMs provides insight to the instabilities, control of ELMs is the ultimate goal. As discussed above, the plasma boundary shape significantly affects the ELM characteristics in NSTX. Active control with externally

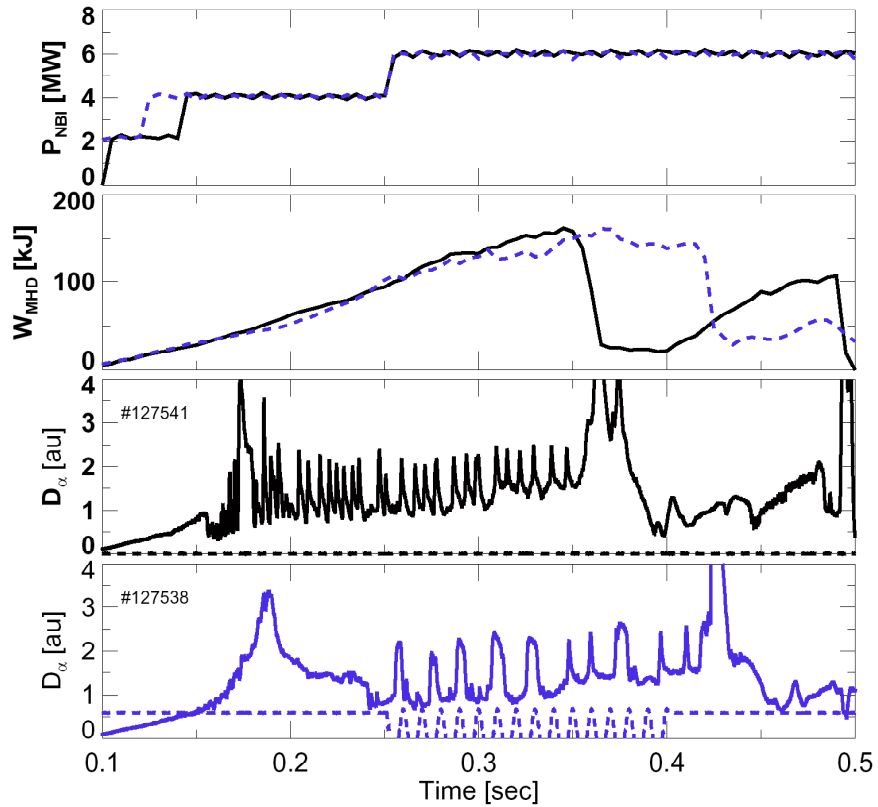


Fig. 5.2.1.7- Comparison of Type I ELMy discharges with (blue) and without n=3 3-D perturbation.

applied non-axisymmetric magnetic perturbations is being tested in NSTX, using a set of 6 midplane window-frame coils external to the vacuum vessel. The goal is to determine if these coils will allow ELM suppression as observed with internal coils in DIII-D⁷¹. Because internal coils could have a significant cost/schedule impact in next step devices, e.g. in ITER, experiments with external coils can help corroborate the need for such coils.

The NSTX coils allow a variety of spectra: pure n=1, pure n=3, mixed n=1+n=3, mixed n=2+n=3, or mixed n=2+n=4. The experimental studies to date have been guided by calculations of the island overlap from application of the 3-D field, both vacuum response and also including plasma response with the IPEC code⁸⁰. Fig. 5.2.1.6 shows

that the Chirikov parameter was expected to exceed 1 for $\psi_N > 0.7$, i.e. for a large region of the edge plasma. This condition (Chirikov > 1 for a large part of the edge plasma) is believed to be necessary for ELM suppression⁸¹. Two sets of studies have been completed: applying a variety of DC and AC fields to a plasma with reproducible, robust Type I ELMs, and applying $n=3$ fields to a plasma with a long ELM-free phase. In the first set of studies, reproducible ELM modification (but not suppression) has been observed. Specifically the Type I ELM signature on D_α is modified: the typical ELM duration of ~ 5 ms duration was doubled to ~ 10 ms, and the frequency was decreased. Data from soft X-rays and fast visible cameras shows that two or more large Type I ELMs are observed to occur within the single 10ms D_α signature, indicating a change in the ELM stability. In the second set of studies, $n=3$ magnetic perturbation was shown to reproducibly de-stabilize ELMs in an otherwise ELM-free period of the discharge, e.g. Fig. 5.2.1.7. In this case, the ELMs have similar signatures to normal Type I ELMs on

various NSTX diagnostics. Edge stability analysis on these discharges is underway. Finally this latter technique was very recently used in conjunction with ELM-free discharges (from Li evaporation), to trigger controlled ELMs (e.g. Fig. 5.2.1.8) and reduce the radiated power.

While ELM and pedestal research has clear overlap, H-mode pedestal studies have a broader goal of the

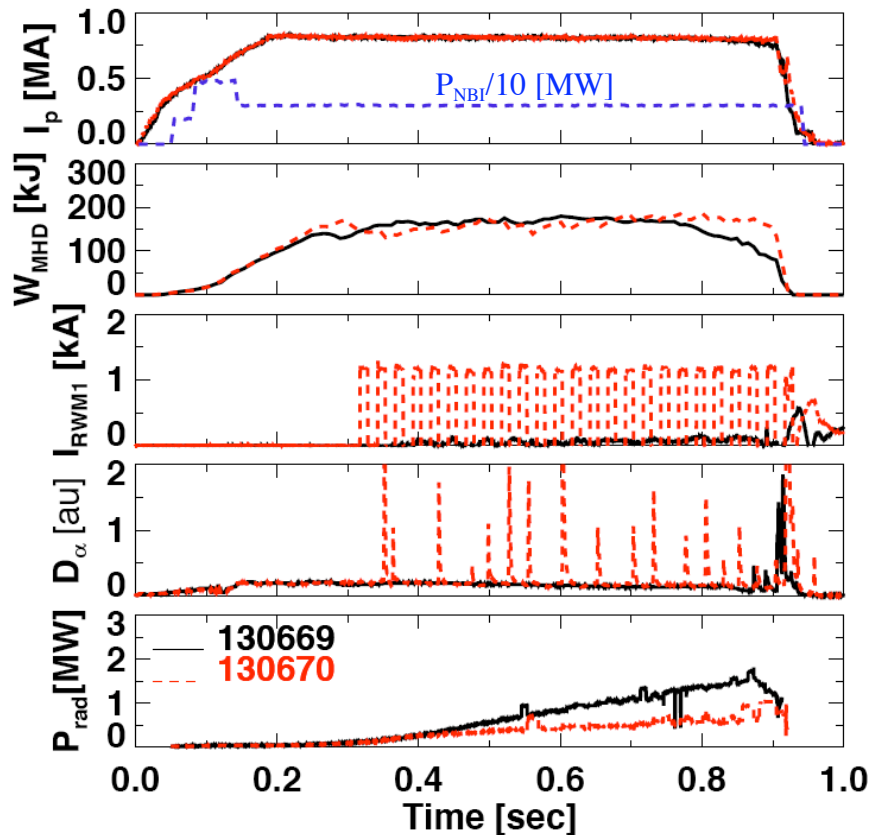


Fig. 5.2.1.8- Comparison of ELM-free discharges with/without $n=3$ perturbation applied. ELMs are triggered by the $n=3$ pulses, reducing the rate of increased in radiated power.

assessment of the dependence of pedestal properties on dimensional and dimensionless parameters. Over the past decade, an analysis technique has been developed to facilitate evaluation of the H-mode pedestal heights, widths and gradients for comparison across devices. The procedure involves fitting plasma density and temperature profiles to a mathematical function which includes a hyperbolic tangent term and a linear term⁸². Typically the NSTX pedestal n_e , T_e , and P_e are in a range between 2 and $5 \times 10^{19} \text{ m}^{-3}$, 100 and 300 eV, and 1 and 3 kPa respectively⁷⁵. The T_i profile is measured by a Charge Exchange Recombination Spectroscopy system; evaluation of the pedestal top is possible for $T_i > 200 \text{ eV}$, as the signal strength drops off strongly below this value. It can be stated that in quasi-steady conditions when both measurements are available, the pedestal T_i is very close to the pedestal T_e , i.e. in the range of a few hundred eV.

The use of lithium wall conditioning to reduce the density has indeed produced an increase in the edge T_e and T_i , as anticipated (see Fig. 5.2.1.9). Because the post-lithium discharges are ELM-free, the edge n_e is actually higher than in the pre-lithium discharges. This the edge pressure gradient increased. One theory for the ELM suppression is that this enhanced pressure gradient leads to higher edge bootstrap current density, which in turn

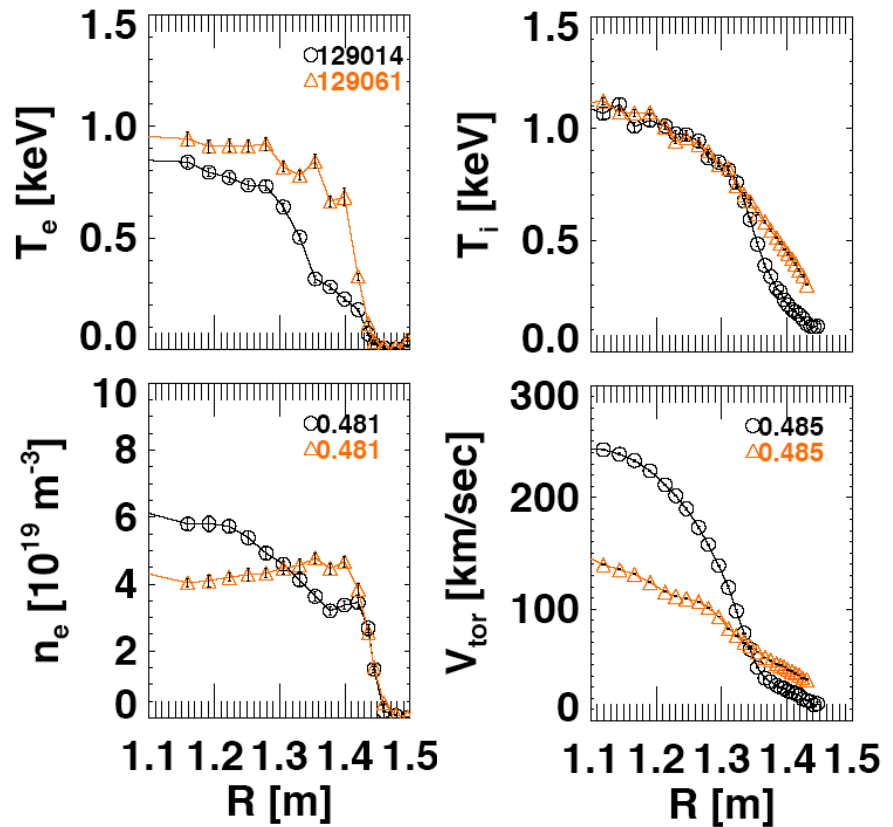


Fig. 5.2.1.9- Comparison of pre-(black) and post-LiTER(orange) discharges with double LiTER system in 2008: $I_p=0.9 \text{ MA}$, $B_t=0.45 \text{ T}$, $P_{\text{NBI}}=4 \text{ MW}$, $\delta=0.8$, $\kappa=2.2$. The drop in core toroidal rotation is not understood.

opens up access to second stability regimes. Tests of hypotheses such as these are in progress.

3. Plans

We plan to assess the edge stability in discharges with the different ELM types shown in [Figure 5.2.1.2](#). The first step in this assessment is to use all of the Thomson channels to constrain the equilibrium fits. The next step is to assess the edge stability with codes such as ELITE⁷⁷ or DCON⁸³, and compare the prediction of the pressure gradient limit to the measured time-dependent pressure gradient. The present analysis is partly limited by 1) the spatial resolution of the n_e and T_e data from Thomson Scattering, 2) the difficulty in obtaining carbon-based charge exchange T_i profiles when $T_i < 200$ eV, and 3) the transient nature of NSTX H-mode discharges which often exhibit a secular density ramp. These limitations will be reduced by enhancing diagnostic capability and improving control tools: 1) additional edge Thomson spatial channels will be added in FY 2009 and available for the F 2010 run, 2) the passive edge rotation diagnostic will be upgraded in both spatial and time resolution, 3) a high spatial resolution ~ 1 ms time response edge Soft X-ray system will be implemented for n_e and T_e profile reconstruction, and 4) density control will improve as the Liquid Lithium Divertor is commissioned and fueling upgrades (high-field side fueling, supersonic gas injector) are implemented. In addition the availability of poloidal CHERs by the beginning of FY 2009 will allow an E_r correction to the edge MSE data to more effectively use it for equilibrium reconstructions used in the edge stability analysis.

The accessibility of the small, Type V ELM in NSTX has increased the NSTX pulse length and performance as compared with Type I ELMy discharges. We plan to continue this research line to answer outstanding questions, e.g.:

- 1) What is the underlying instability responsible for the Type V ELM? Is it an ideal or a resistive mode?
- 2) How far can the regime be extended in v_*^e space in NSTX, i.e. what is the dependence of the v_*^e threshold for Type V and Mixed regimes on δ_r^{sep} , δ , and κ ?

- 3) What is the significance of the apparent threshold of the Mixed regime onset with the global parameter β_N ? Is the correlation actually with pedestal β , which probably scales with β_N ?
- 4) Has the regime been observed in other devices? If not, is the regime extensible to other devices?

Question #2 above is the subject of an ITPA experiment in which NSTX is participating, in collaboration with the MAST and ASDEX-Upgrade devices. Question #4 is the subject of a second collaborative experiment to assess the commonality of small ELM regimes between the NSTX, Alcator C-MOD, and MAST devices. We anticipate that these studies will be completed FY09-10. The new diagnostics described above will contribute to these studies by allowing a more quantitative assessment of the edge profiles as the different ELM regimes are encountered.

While suppression of ELMs with magnetic perturbations has not been achieved, the edge stability can clearly be altered. The path to ELM suppression may well require reduced collisionality, which is the goal of the LLD program, and/or a broader poloidal mode spectrum. Hence additional attempts at ELM suppression with the existing midplane coils will be made after reduced density discharges have been developed with the LLD. In addition, detailed experiments to understand the change in edge stability caused by these perturbations, including when ELMs are de-stabilized, will be completed.

The prospects of ELM stabilization (or de-stabilization as needed in ELM-free discharges from Li coatings) will be improved by the planned upgrade to the EFCC system. In the baseline budget, adding a second set of switching power amplifiers (SPAs) will allow feedback control for $n=1$ and $n=3$ modes *while applying* an $n=2+4$ perturbation, which has shown the most promise for creating an ergodic edge region for ELM suppression studies. This capability is not possible with the present set of three SPAs. In the incremental budget, new internal non-axisymmetric control coils will allow imposition of up to pure $n=6$ fields with more control over the poloidal mode spectrum. These coils will allow more precise localization of the perturbation to the edge, avoiding excessive rotation drag from lower- n perturbations. The technical details of these upgrades are given in the facility chapter 7.

We also plan to characterize the H-mode pedestal in detail, in particular the dependence of the heights, widths, and gradients on 1) control parameters, such as I_p , B_t , P_{NBI} , P_{RF} , n_e , etc., and 2) dimensionless parameters, such as v_{\square}^* and ρ^* . Completion of the multi-machine experiment between NSTX, DIII-D, and MAST to determine the dependence of the pedestal on aspect ratio is a high priority item. Here the improved spatial resolution of the Thomson Scattering, the new high-resolution edge Soft X-ray system, and improved Edge Rotation Diagnostic are critical to an accurate experimental determination of the pedestal heights, widths and gradients.

Although there are presently few theory tools with which to compare these measurements, development of the XGC neoclassical transport code³⁹ will continue and we anticipate detailed comparisons with code predictions over the next few years. The present version (XGC-0) requires the stipulation of anomalous transport coefficients in addition to the neoclassical ones. The version in development (XGC-1) will compute the transport from an advanced turbulence model. The code predictions will be used not only to test pedestal dependencies on various parameters, but also how the pedestal evolves both between ELMs and leading up to the ELM crash.

5.2.2 H-mode transition physics

1. Introduction

H-mode discharges are important for the NSTX program because: 1) H-modes are characterized by broad pressure profiles, and therefore higher ideal stability limits; and 2) the edge pressure gradient drives bootstrap current, leading to a higher non-inductive current fraction, and therefore longer discharge pulse lengths. H-mode access is usually observed above a critical input power, known as the L-H power threshold (P_{LH}). Development of models to predict P_{LH} for extrapolation has been an active research topic since the discovery⁸⁴ of the H-mode in the early 1980's. NSTX can contribute to H-mode transition physics in several critical ways. Here we discuss three areas: 1) dependence of P_{LH} on discharge boundary shape, 2) dependence of P_{LH} on heating mechanism, i.e. NBI vs. RF heating, and 3) dependence of P_{LH} on fueling location and mechanism.

Many details of the underlying physics of the H-mode transition have yet to be ascertained. External heating methods, e.g. NBI, complicate the determination of the fundamental physics because of the additional particle and momentum source, and so investigating L-H transitions with ohmic heating power alone provides additional insight. One important question is the level of change in core turbulence, which accompanies the development of the edge transport barrier. A simultaneous measurement of the edge and core fluctuations and correlation lengths can be obtained in ohmic H-modes because the density profile remains centrally peaked for a modest period of time after the transition. In NBI H-modes, the edge density rises quickly, preventing measurement of the core turbulence correlation length with reflectometry.

2. Background and results

Historical studies of the power threshold have identified the plasma surface area, the toroidal field, and the plasma density as the critical control parameters⁸⁵. Recently, the role of boundary shape was re-investigated, and it was concluded that P_{LH} exhibited a minimum value in balanced double-null configuration in the MAST device⁸⁶.

The shape experiment was repeated in NSTX, with participation from scientists from MAST. The results were rather similar: the P_{LH} with NBI fueling was lowest in a DN

shape, doubling in LSN shape and doubling again in USN shape⁸⁷ (e.g. Fig. 5.2.2.1). These results were extended further to plasmas with RF heating; the rationale was that whereas 1/3 of the NB heating goes directly to the ions, RF heats the electron population. In addition, NBI imparts momentum whereas RF does not. This comparison was intended to highlight the roles of electron/ion heat flux and rotation on P_{LH} .

It was found, however, that the P_{LH} local minimum in the DN shape was present with either heating method. Moreover, P_{LH} increased as the discharge shape was made to favor the lower divertor even more, i.e. when δr_{sep}^{sep} was reduced further. It was also found that P_{LH} was comparable with either RF or NBI heating. Note that the core plasma profiles differed substantially, but the edge profiles were nearly identical at constant density.

Other power threshold studies⁸⁸ have

suggested that neutrals and fueling play an important role in the actual value of P_{LH} . Further experiments highlighted a dependence on the gas fueling rate: discharges with low gas fueling and no NBI heating during the plasma current ramp showed comparable

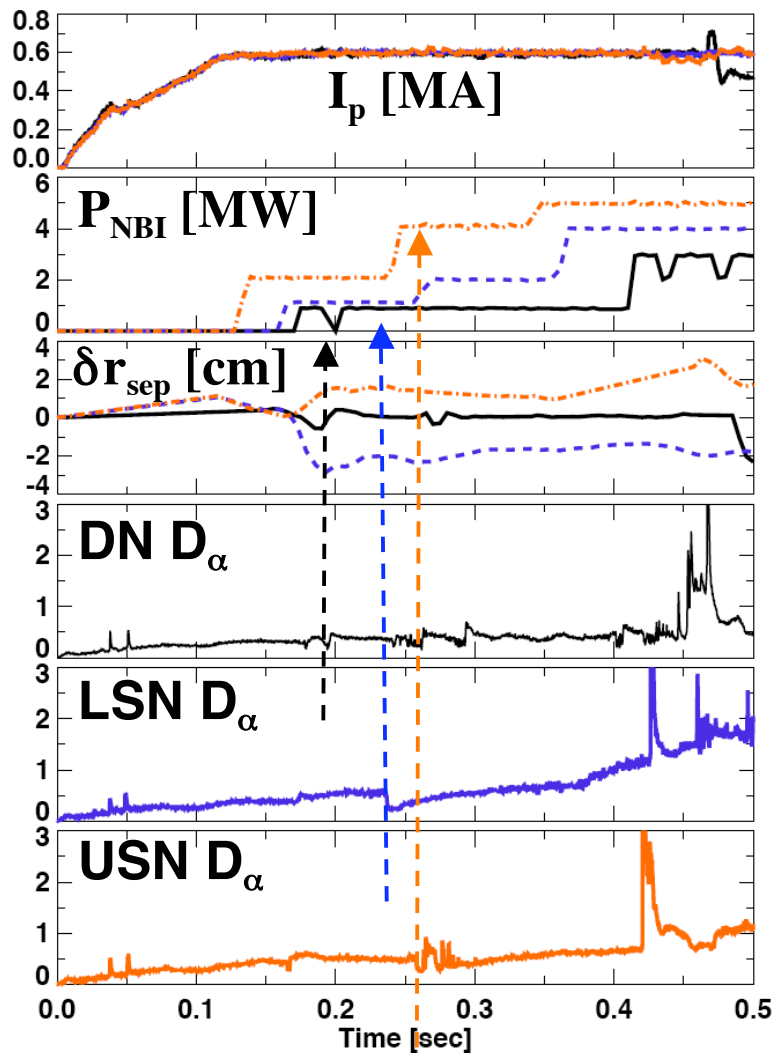


Fig. 5.2.2.1- Comparison of L-H power threshold for balanced double-null (black), lower single-null (blue) and upper single-null (orange).

L-H transition powers for HFS midplane and LFS midplane fueling⁷⁵. Finally, research to date shows that the correlation length for turbulent density fluctuations in the core of ohmic plasmas to decrease 50-75% across the L-H transition⁸⁹. In some cases there is a spontaneous spin up of both edge intrinsic poloidal and toroidal rotations prior to the transition itself.

There are few quantitative theories with which to compare these observations. Recently a new theory (the gyrocenter shift GCS theory) was developed to explain the mechanism of formation of the radial electric field (E_r) at the tokamak boundary. The origin of E_r remains one of the most important problems in L-H transition physics. The basic concept behind GCS is that the neutral density radial gradient in the edge leads to a gradient in the charge exchange rate, hence a radial current and an E_r (see fig. 5.2.2.2). The validity of GCS theory was tested both in low temperature plasmas⁹⁰ and for NSTX directly⁹¹. This theory might clarify the physics of L-H transition by uncovering the mechanism behind a transition from turbulent flow to laminar flow⁹².

3. Plans

Thorough analysis of existing data is the first step. From the previously run L-H experiments, the discharges will be analyzed with the TRANSP code to obtain the heat flux in the separate and ion channels, to see if they

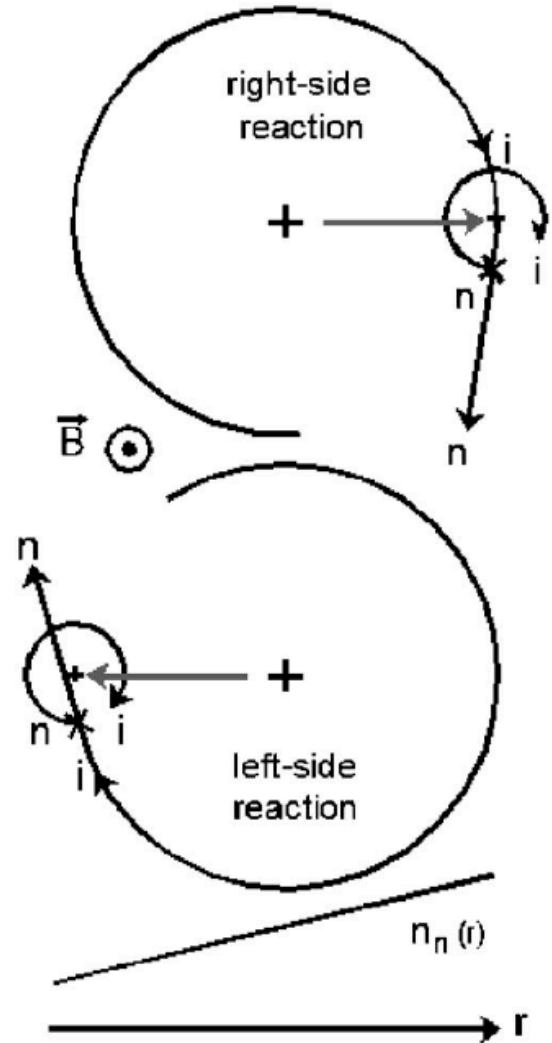


Fig. 5.2.2.2- Schematic of gyrocenter shift originating from charge exchange reactions. The charge exchange rate is higher on the right hand side than the left hand side because of the neutral density gradient, leading to a radial current and radial electric field (E_r) buildup.

actually differed with RF and NBI heating. Although the core n_e , T_e , T_i and v_ϕ differed in the RF and NBI discharges, collisional coupling may have forced the edge heat flux distribution between electrons and ions to be similar.

From 2009-2011, we plan to assess the dependence of the power threshold on other shape quantities as well, namely the δ and κ , as discharges with variations in these two parameters have exhibited different H-mode access conditions in uncontrolled experiments. The effect of rotation on P_{LH} will also be measured, as ITER is expected to have low rotation speed. We also propose to complete the dependence of P_{LH} on external parameters, such as B_t and the fueling rate. We note that past power threshold experiments have been unable to test the E X B shear stabilization paradigm because one component in the radial force balance, the poloidal rotation v_θ , was not measured by the existing CHERs system. A new poloidal CHERs system was recently installed on NSTX during 2007, and it will enable calculation of the E_r profiles to compare with the E X B shearing rate to further test the E X B paradigm.

We also plan to complete the previous study concerning the effect of the poloidal fueling location on P_{LH} . Several new capabilities have appeared since the last study: 1) a new supersonic gas injector, which allows reproducible H-mode access with LFS fueling in NSTX for the first time; 2) the availability of poloidal CHERs; and 3) continued improvement of the plasma control system, allowing improved position control for improved diagnostic measurements.

Following the center stack upgrade in 2011, we will extend the empirical scalings of P_{LH} to higher I_p and B_t , i.e. closer to next generation STs. Also in this longer term time frame, we plan to perform a more rigorous test of the GCS theory and its impact on the L-H transition and power threshold. Such a test requires a large number of diagnostics, and most of the required diagnostics⁹³ will be available during FY11-13. In particular, measurement of neutral density profile is one of the most important parameters in the gyrocenter shift theory, and techniques are being developed to make these measurements in the X-point region. We also plan to make comparisons with numerical simulations of these data with the XGC code.

Chapter 5 References

- 1 J. E. Menard, et. al., *Nucl. Fusion* **47** (2007) 645.
- 2 D. K. Mansfield, et. al., *Nuclear Fusion* **41** (2001) 1823.
- 3 R. Budny, et. al., *J. Nucl. Materials* **196-198** (1992) 462.
- 4 S. V. Mirnov, et. al., *Fus. Eng. Des.* **65** (2003) 455.
- 5 V. Evitkin, et. al., *Fus. Eng. Des.* **56-57** (2001) 363.
- 6 R. Majeski, et. al., *Physical Review Letters* **97** (2006) #075002.
- 7 H. W. Kugel, et. al., *Physics of Plasmas* **15** (2008) #056118.
- 8 D. K. Mansfield, et. al., *J. Nucl. Materials* (2008) submitted.
- 9 R. Maingi, et. al., *Plasma Physics Controlled Fusion* **46** (2004) A305.
- 10 A. R. Field, et. al., *Plasma Physics Controlled Fusion* **46** (2004) 981.
- 11 V. A. Soukhanovskii, et. al., *Rev. Sci. Instrum.* **75** (2004) 4320.
- 12 V. A. Soukhanovskii, et. al., *Proc. 21st IEEE/NPSS Symposium on Fus. Eng., Knoxville, TN, Sep. 26-29* (2005) 2005.
- 13 V. A. Soukhanovskii, et. al., *Proc. 22nd IEEE Symposium on Fus. Eng., Albuquerque, NM June 17-21* (2007).
- 14 L. Yao, et. al., *Nucl. Fusion* **41** (2001) 817.
- 15 B. Pegourie, et. al., *J. Nucl. Materials* **313-316** (2003) 539.
- 16 P. T. Lang, et. al., *Plasma Phys. Contr. Fusion* **47** (2005) 1495.
- 17 V. A. Soukhanovskii, et. al., *Proc. 2008 Euro. Conf. on Plasma Phys. and Contr. Fusion, London, U.K.* **ECA 28G** (2004) paper P2.190.
- 18 V. A. Soukhanovskii, et. al., *Proc. 2006 Euro. Conf. on Plasma Phys. and Contr. Fusion, Roma, Italy* **ECA 30G** (2006).
- 19 V. A. Soukhanovskii, et. al., *Proc. 2008 Euro. Conf. on Plasma Phys. and Contr. Fusion, Crete, Greece* **ECA 32G** (2008).
- 20 D. P. Stotler, et. al., *J. Nucl. Mater.* (2008) submitted.
- 21 R. Kaita, et. al., *Physics of Plasmas* **14** (2007) #056111.
- 22 P. Staib, et. al., *J. Nucl. Materials* **111-112** (1982) 109.
- 23 W. Fundamenski, et. al., *Fusion Science Techn.* **53** (2006) 1023.
- 24 T. D. Rognlien, et. al., *Journal of Nuclear Materials* **196-198** (1992) 347.
- 25 R. Schneider, et. al., *Contrib. Plasma Physics* **46** (2006) 3.
- 26 J. W. Ahn, et. al., *Phys. Plasma* (2008) submitted.
- 27 R. J. Maqueda, et. al., *Review of Scientific Instruments* **72** (2001) 931.
- 28 S. J. Zweben, et. al., *Nuclear Fusion* **44** (2004) 134.
- 29 S. J. Zweben, et. al., *Physics of Plasmas* **13** (2006) 056114.
- 30 J. A. Boedo, et. al., *Plas. Phys. Contr. Nuclear Fusion Res.* (2006) paper EX/6.
- 31 J. R. Myra, et. al., *Phys. Plasma* **13** (2006) #092509.
- 32 J. R. Myra, et. al., *Plas. Phys. Contr. Nuclear Fusion Res.* (2006) paper TH/P6.
- 33 J. R. Myra, et. al., *Proc. 21st Fusion Energy Conference, Chengdu, China, Oct. 16-21, 2006* (2006) paper TH/P6.
- 34 R. Maingi, et. al., *J. Nucl. Materials* **363-365** (2007) 196.
- 35 R. Maingi, et. al., *Proc. 2007 Euro. Conf. on Plasma Phys. and Contr. Fusion, Warsaw, Poland, July 2-6, 2007* (2007) paper P2.020.
- 36 A. I. Shestakov, et. al., *J. Comput. Phys.* **85** (2003) 399.

- 37 T. D. Rognlien, et. al., *J. Nucl. Materials* **337-339** (2005) 327.
38 T. D. Rognlien, et. al., *Contrib. Plasma Phys.* **44** (2004) 188.
39 C. S. Chang, et. al., *Physics of Plasmas* **11** (2004) 2649.
40 D. D. Ryutov, et. al., *Plasma Phys. Contr. Fusion* **43** (2001) 1399.
41 S. J. Zweben, et. al., *J. Nucl. Materials* (2008) submitted.
42 D. A. D'Ippolito, et. al., *Phys. Fluids B* **5** (1993) 3603.
43 Y.-K. M. Peng, et. al., *Plasma Physics Controlled Fusion* **47** (2005) B263.
44 V. A. Soukhanovskii, et. al., *J. Nucl. Materials* **337-339** (2005) 475.
45 R. Maingi, et. al., *Journal of Nuclear Materials* **313-316** (2003) 1005.
46 R. Maingi, et. al., *J. Nucl. Materials* **363-365** (2007) 196.
47 K. Borass, et. al., *Nuclear Fusion* **31** (1991) 1035.
48 R. Maingi, et. al., *Plasma Physics Controlled Fusion* **45** (2003) 657.
49 R. Maingi, et. al., *Nuclear Fusion* **43** (2003) 969.
50 S. F. Paul, et. al., *J. Nucl. Materials* **337-339** (2005) 251.
51 D. A. Gates, et. al., *Physics of Plasmas* **13** (2006) #056122.
52 V. A. Soukhanovskii, et. al., *J. Nucl. Materials* **363-365** (2007) 432.
53 V. A. Soukhanovskii, et. al., *Proc. 21st Fusion Energy Conference, Chengdu, China, Oct. 16-21, 2006* (2006) paper EX/P4.
54 V. A. Soukhanovskii, et. al., *Phys. Plasma* (2008) to be submitted.
55 R. Goswami, et. al., *Phys. Plasma* **8** (2001) 857.
56 D. P. Stotler, et al., et. al., *Contribution to Plasma Physics* **44** (2004) 294.
57 P. C. Stangeby, *The Plasma Boundary of Magnetic Fusion Devices* (IoP, Toronto, 2000).
58 D. D. Ryutov, et. al., *Phys. Plasma* **14** (2007) #064502.
59 A. W. Leonard, et. al., *J. Nucl. Materials* **266-269** (1999) 109.
60 A. Loarte, et. al., *Plasma Physics Controlled Fusion* **45** (2003) 1549.
61 G. Federici, et. al., *J. Nucl. Materials* **313-316** (2003) 11.
62 T. Ozeki, et al., et. al., *Nuclear Fusion* **30** (1990) 1425.
63 J. Stober, et. al., *Nuclear Fusion* **41** (2001) 1123.
64 G. Saibene, et. al., *Nuclear Fusion* **45** (2005) 297.
65 A. W. Leonard, et. al., *J. Nucl. Materials* **290-293** (2001) 1097.
66 G. Saibene, et. al., *Plasma Physics Controlled Fusion* **44** (2002) 1769.
67 Y. Kamada, et. al., *Plasma Physics Controlled Fusion* **42** (2000) A247.
68 Y. Takase, et. al., *Physics of Plasmas* **4** (1997) 1647.
69 K. Kamiya, et. al., *Nuclear Fusion* **43** (2003) 1214.
70 C. M. Greenfield, et. al., *Physical Review Letters* **86** (2001) 4544.
71 T. E. Evans, et. al., *Physical Review Letters* **92** (2004) article #235003.
72 P. B. Snyder, et. al., *Physics of Plasmas* **12** (2005) 056115.
73 R. Maingi, et. al., *Physics of Plasmas* **13** (2006) #092510.
74 R. Maingi, et. al., *J. Nucl. Materials* **337-339** (2005) 727.
75 R. Maingi, et. al., *Nuclear Fusion* **45** (2005) 1066.
76 R. Maingi, et. al., *Nuclear Fusion* **45** (2005) 264.
77 P. B. Snyder, et. al., *Physics of Plasmas* **9** (2002) 2037.
78 P. B. Snyder, et. al., *Plasma Physics Controlled Fusion* **46** (2004) A131.
79 R. Maingi, et. al., *Proc. 21st Fusion Energy Conference, Chengdu, China, Oct. 16-21, 2006* (2006) paper IT/P1#12.

- 80 J.-K. Park, et. al., *Phys. Plasma* **14** (2007) #052110.
81 M. E. Fenstermacher, et. al., *Phys. Plasma* **15** (2008) #056122.
82 R. J. Groebner, et. al., *Plasma Physics Controlled Fusion* **40** (1998) 673.
83 A. H. Glasser, et. al., *Bull. Am. Phys. Soc.* **42** (1997) 1848.
84 F. Wagner, et. al., *Physical Review Letters* **49** (1982) 1408.
85 J. A. Snipes, et. al., *Proc. of the 19th International Conference on Plasma Physics
and Controlled Fusion, Lyon 2002 (IAEA, Vienna) (2002) paper CT/P#04.*
86 H. Meyer, et. al., *Plasma Physics Controlled Fusion* **46** (2004) A291.
87 T. M. Biewer, et. al., *Proc. 33rd EPS Conference on Plasma Physics and Contr.
Fusion, Roma, Italy, June 19-23, 2006 (2006) Paper 5.112.*
88 B. A. Carreras, et. al., *Physics of Plasmas* **5** (1998) 2623.
89 C. E. Bush, et. al., *Presented at the 11th US-EU TTF Workshop, Marseille,
France, Sept. 4-7, 2006 (2006).*
90 K. C. Lee, et. al., *Phys. Plasma* **13** (2006) #062505.
91 K. C. Lee, et. al., *Phys. Plasma* (2008) to be submitted.
92 K. C. Lee, et. al., *Nucl. Fusion* (2008) to be submitted.
93 K. C. Lee, et. al., *Rev. Sci. Instrum.* **77** (2006) 10F505.

This page intentionally left blank